For Polymer Journal Rising Stars -2021-

PPV-Type π-Conjugated Polymers Based on Hypervalent Tin(IV)-fused Azobenzene Complexes Showing Near-Infrared Absorption and Emission

Masayuki Gon, Kazuya Tanimura, Misao Yaegashi, Kazuo Tanaka and Yoshiki Chujo*

Department of Polymer Chemistry, Graduate School of Engineering, Kyoto University Katsura, Nishikyo-ku, Kyoto 615-8510, Japan

E-mail: tanaka@poly.synchem.kyoto-u.ac.jp

Key words: tin; conjugated polymer; hypervalent; near-infrared; azobenzene

Abstract

We demonstrate NIR-absorptive and emissive poly(*p*-phenylene vinylene) (PPV) type π-conjugated polymers based on hypervalent tin-fused azobenzene (TAz) complexes. Taking advantage of inherent narrow-energy-gap of TAz complexes originating from the three-center four-electron (3c-4e) bond and the nitrogen–tin (N–Sn) coordination, the synthesized polymers, TAz-PPVs, showed absorption and emission in the wavelength regions over 750 nm and 810 nm in diluted solution, respectively. From the experimental and theoretical investigations, it was shown that elevation of highest occupied molecular orbital (HOMO) and reduction of lowest unoccupied molecular orbital (LUMO) were simultaneously caused by extension of π-conjugation. The effective conjugation length was calculated to be $n>10$ (n: degree of polymerization) and the value was comparable to conventional PPV systems. Through this research, we revealed that π-conjugated systems including hypervalent bonds were able to expand the π-conjugation. According to the concept of "element-blocks", development of heteroatom-containing narrow-energy-gap monomers should be novel approaches for construction of bland new NIR-absorptive and emissive materials.

1. Introduction

Because of unique physical properties of near-infrared (NIR) light, such as invisibility and high permeability in various media, NIR-absorptive and emissive substances are versatile in a wide variety of applications, such as developments of security inks, night vision cameras, bioimaging probes, sensors, and optical communication media[1–8]. To realize future technologies relating with NIR light, not only photochemical functions but also material properties, such as processability and solubility in conventional media, are essential. Although several types of organic dyes have been developed as a scaffold for NIR materials, many researchers have still explored new molecular skeletons for obtaining NIR properties to meet increasing demands in the development of advanced devices, such as film-type organic light emitting devices (OLEDs), organic photovoltaics (OPVs), selective bioimaging and photoacoustic imaging (PAI)[9–20]. Most of difficulties in the design of NIR-absorptive and emissive materials are caused from the limited extension of conjugation length[21–23]. Therefore, it is of great significance to establish a novel design strategy for realizing narrow energy gaps without extension of π-conjugation systems[24–27].

We recently proposed the concept of "element-blocks", which are structural functional units composed of various groups of elements, to produce advanced materials[28–30]. As examples of "element-blocks", we have discovered that cubic silica and boron cluster compounds named polyhedral oligomeric silsesquioxane (POSS)[31–33] and *o*-carborane[34,35], respectively, have a potential to apply to superior luminescent materials with high durability and stimuli-responsiveness. By using this concept, various types of heteroatom-containing π-conjugated building blocks have been developed[36–40]. More recently, we have reported that boron-fused

azobenzene/azomethine (BAz/BAm) complexes, which are “boron element-blocks”, worked as unique functional building blocks[41–51]. For example, by using strong electron-accepting ability of BAz and BAm complexes, the π-conjugated polymers with highly efficient emission from visible to NIR region both in solution and film states were able to be prepared by construction of donor–acceptor (D–A) systems[42–45]. Furthermore, poly(*p*-phenylene vinylene) (PPV) type π-conjugated copolymers composed of alternating BAz and vinylene units (BAz-PPV) showed NIR-absorptive and emissive properties[46]. These functions should be caused from effective connection of the π-conjugated system having inherent narrow energy gap of the BAz moiety via vinylene units. These results indicate the potential of aza-substituted PPV systems[52] assisted by heteroatom coordination for NIR dyes, despite that conventional PPVs consisting of carbon–carbon double (C=C) bonds show yellow to orange-color absorption and emission[53–59]. Additionally, PPVs are one of conventional polymers for fabricating OLEDs and OPVs because of excellent luminescence and high carrier mobility[60–63]. Thus, PPV-based molecular designs for optically functional polymers are advantageous for constructing practical devices in the future applications.

Herein, we focused on tin-fused azobenzene (TAz) complexes for inducing narrower energy gaps by the coordination to the azobenzene moiety in the aza-substituted PPV system. Recently, we showed that it is possible to form the hypervalent state in the TAz complex having five-coordinated distorted trigonal bipyramidal geometry[64]. In particular, we discovered that the TAz complexes have absorption and emission bands in the longer wavelength regions (absorption: ~550 nm, emission: ~680 nm)[65,66] than the BAz complexes (absorption: ~530 nm, emission:

~640 nm) [44–46] despite that only boron was replaced to tin in the heteroatom-fused azobenzene complex moieties. The quantum calculation data suggested that the large absorption band should be attributed to the combinational electronic interactions from the hypervalent tin atom which has an electron-donating three-center four-electron (3c-4e) bond at apical positions and an electron-accepting nitrogen–tin (N–Sn) coordination at equatorial positions[64]. On the basis of this unique electronic properties of the hypervalent tin atom, we designed the PPV-type π-conjugated polymers involving the TAz complexes (TAz-PPV) to achieve larger absorption and emission properties in the longer wavelength region than BAz-PPV (Figure 1). Finally, we accomplished to obtain the TAz-PPV polymers which can exhibit NIR-absorptive and emissive properties in the wavelength region over 750 and 810 nm, respectively. To the best of our knowledge, these data firstly indicate that introduction of hypervalent element can effectively perturb the electronic structure of main-chain conjugation of polymers followed by narrow energy gaps, similarly to extension of π-conjugated system as well as combinational substituent effects with electron-donating and withdrawing groups. Therefore, our approach is expected to be a bland new strategy to obtain NIR-absorptive and emissive materials based on conjugated polymers.

Figure 1

2.1 Synthesis

The synthetic method of TAz derivatives is shown in Scheme 1. 2-Octyldodecyl groups were introduced for enhancing solubility of the products to common organic solvents, such as chloroform, dichloromethane, tetrahydrofuran, and toluene. The brominated methoxy azobenzene derivative (**1-Br**) was prepared according to the previous literature[46]. Deprotection of methyl groups of **1-Br** was executed by boron tribromide (BBr_3) to afford an O,N,O-type tridentate ligand (**2-Br**) in 76% isolated yield. Then, condensation reaction with **2-Br** and diphenyltin(IV) oxide (Ph_2SnO) or dioctyltin(IV) oxide ($(C_8H_{17})_2SnO$) was carried out in acetone at reflux temperature to provide **TAz-Ph-Br** or **TAz-C8-Br** in quantitative isolated yields, respectively. As the non-brominated monomeric units, **TAz-Ph-H** and **TAz-C8-H** were synthesized by the same method from the non-brominated methoxy azobenzene derivative (**1-H**). Next, **TAz-Ph-Br** and **TAz-C8-Br** were used for polymerization with a vinylene co-monomer (Scheme 2). Concretely, Migita–Kosugi–Stille cross-coupling polymerizations[66,67] with **TAz-Ph-Br** or **TAz-C8-Br** and *trans*-1,2-bis(tributylstannyl)ethylene (**3**) were executed in a catalytic system involving $Pd_2(dba)_3$ (dba = dibenzylideneacetone) and 2-dicyclohexylphosphino-2′,4′,6′-triisopropylbiphenyl (XPhos) to afford target copolymers, **TAz-PPV-Ph** or **TAz-PPV-C8**, in 80% and 60% isolated yields, respectively.

Scheme 1 and 2

The number and weight average molecular weights (M_n and M_w) of the obtained polymers were calculated to be M_n = 9,500, M_w = 30,300 (M_w/M_n = 3.2) for

TAz-PPV-Ph and M_n = 4,600, M_w = 11,000 (M_w/M_n = 2.4) for **TAz-PPV-C8** by gel permeation chromatography (GPC) with polystyrene standards. All synthesized compounds were characterized by ^{1}H, ^{13}C, ^{119}Sn NMR, and mass spectra (see the Supplementary Information) and showed good solubility in above-mentioned organic solvents. In contrast to the monomers, the clear peaks were not obtained in ^{119}Sn NMR spectra from the polymers. Therefore, we confirmed the existence of repeating units of **TAz-PPV-Ph** or **TAz-PPV-C8** by a MALDI-TOF MS measurement. From those characterization data, we concluded that the products have the expected structures and enough purity for further analyses.

To evaluate the effect of expanding π-conjugation in detail, the synthesized polymers were fractionated by molecular weight with high performance liquid chromatography (HPLC). The results are summarized in Figure S1 and Tables 1, S1 and S2. **TAz-PPV-Ph** and **TAz-PPV-C8** were separated as six and seven fractions of M_n = 6,000~41,000 (M_w/M_n = 1.5~2.2) and M_n = 2,200~29,000 (M_w/M_n = 1.2~1.4), respectively.

Table 1

2.2 Optical measurements

First, we measured optical properties of the synthesized TAz derivatives to evaluate the effect of the expansion of π-conjugation on electronic structures in the ground state (Table 1). Figure 2 shows UV–vis–NIR absorption spectra of fractionated TAz polymers and monomeric units, **TAz-Ph-H** and **TAz-C8-H**, in the diluted chloroform solutions. The gradual bathochromic shifts of maximum absorption

wavelengths (λ_{abs}s) were observed as increasing degree of polymerization (DP, *n*), and finally, the absorption wavelengths reached the NIR region (Figures 2A, 2B, and 2D). This result indicates the hypervalent atom can contribute to the expansion of π-conjugation and the perturbation to conventional π-conjugated systems. The effective conjugation length was estimated to be $n>10$ by a plot of maximum absorption energy versus $1/n$ (Figure 2C). The value was almost similar to the effective conjugation length of the PPV system ($n=8$) evaluated by using oligomeric approaches[54]. In contrast, the value was shorter than $n>50$ in **BAz-PPV** reported in our previous work[46]. Generally, high co-planarity enhances the overlap of aromatic π-orbitals and increases the effective conjugation length. However, interestingly, our results indicate that the waving and flexible units by BAz derivatives (dihedral angle of azobenzene ≈ 165°)[41,45] might be suitable for expansion of effective conjugation length in comparison to the rigid and planar units by TAz derivatives (dihedral angle of azobenzene ≈ 180°)[64] (Figure S2). Further investigation was carried out in the theoretical calculation section. Taking advantage of narrow energy gap of the monomeric units (λ_{abs} ≈ 570 nm), **TAz-PPV-Ph** (λ_{abs} = 756 nm) and **TAz-PPV-C8** (λ_{abs} = 752 nm) had about 50 nm larger λ_{abs}s than **BAz-PPV** (λ_{abs} = 702 nm, monomeric unit: λ_{abs} = 507 nm)[46]. Another interesting feature of the polymerization is that normalized absorbances around 350 nm of TAz derivatives gradually decreased and broadened as increasing DP. Focusing on substitution effect at the tin atom, slightly a larger bathochromic shift of the absorption wavelength was observed in **TAz-C8-H** and **TAz-PPV-C8** than in **TAz-Ph-H** and **TAz-PPV-Ph** at the same molecular weight.

Figure 2

Next, we evaluated photoluminescence (PL) spectra of TAz polymers and monomeric units in chloroform. The obtained spectra are shown in Figure 3. Bathochromic shifts of the maximum PL wavelengths (λ_{PL}s) were monitored as rising the value of DP similarly to the absorption behavior, and eventually the λ_{PL} reached over 810 nm. In addition, the shapes of spectra became sharper as increasing DP and the distinct vibrational structure clearly appeared. Furthermore, Stokes shifts (ν) gradually became smaller by polymerization. These data indicate that expansion of π-conjugation increases rigidity of the π-conjugated system, followed by enhancement of electronic interaction through polymer main chains. The absolute PL quantum efficiency (Φ_{PL}) was not high (Φ_{PL} = 1~2%) and that was slightly enhanced by extension of π-conjugation. Interestingly, the value of Φ_{PL} was gradually decreased as increasing DP. This might be attributed to energy gap law critically observed in NIR region[68–70] and excessive extension of π-conjugation over effective conjugation length or exciton diffusion length[71]. Significant substituent effects at tin were hardly observed, while octyl substituted complexes (**TAz-C8-H** and **TAz-PPV-C8**) showed higher Φ_{PL}s, smaller Stokes shifts and shorter λ_{PL}s than phenyl substituted ones (**TAz-Ph-H** and **TAz-PPV-Ph**). The λ_{PL} of **BAz-PPV** (760 nm) was smaller than that of TAz-PPV derivatives and Φ_{PL} of **BAz-PPV** (2.0%) was comparable to that of TAz-PPV ones[46]. Owing to the narrow-energy-gap monomer, deep NIR absorptive and emissive π-conjugated polymers can be obtained.

Figure 3

2.3 Cyclic voltammetry

To obtain further information of the π-conjugation effect on electronic states, we estimated energy levels of molecular orbitals (MOs) with a cyclic voltammetry (CV). The HOMO and LUMO energy levels were calculated from the onset of the oxidation and reduction curves, respectively (HOMO: highest occupied molecular orbital, LUMO: lowest unoccupied molecular orbital)[72,73]. The results of electrochemical properties are summarized in Table 2 and Figure 4. The cyclic voltammograms are shown in Figure S3. In polymers, higher HOMO and lower LUMO energy levels were obtained than those in monomers, clearly representing that π-conjugation is effectively expanded through the polymer main chains[74,75]. In our previous work, HOMO and LUMO energy levels of BAz-PPV were −5.58 and −3.98 eV, respectively, and the energy gap was calculated to be 1.60 eV[46]. In this study, it was indicated that the narrower energy gaps of TAz-PPV derivatives (1.34 and 1.36 eV) were obtained and largely attributed to the elevation of HOMO energy level (−5.21 and −5.15 eV). This means that electron-donating ability originating from the 3c-4e bond should effectively work even in the expanded π-conjugated system. Notably, focusing on the substituent effect of tin atom, it was revealed that electron donation from alkyl chain increased in both HOMO and LUMO energy levels. These results also indicate that unique electronic interaction of hypervalent tin atom, such as elevation and reduction of HOMO and LUMO, is applicable in main-chain conjugation through conjugated polymers.

Table 2 and Figure 4

2.4 Theoretical calculation

To elucidate the relationship between expansion of π-conjugation and energy gaps, we carried out theoretical calculation with density functional theory (DFT) and time dependent DFT (TD-DFT). Computational details are shown in the Supplementary Information. We used monomers (M), dimers (D), and trimers (T) of **TAz-PPV-Ph′** and **TAz-PPV-C8′** in which the long alkyl chains were replaced with methyl groups to reduce the calculation cost for precise evaluation of the expanded π-conjugated system. The results and the structures are shown in Figure 5. Kohn–Sham orbitals (HOMO and LUMO) are described in Figures S4 and S5. The energy gaps were gradually narrowed by the extension of π-conjugation in the order of monomers, dimers, and trimers (Figure 5A). The influence on energy gaps was larger from monomer to dimer than that from dimer to trimer, implying existence of saturation of the conjugation length. Our experimental results show the effective conjugation length about n=10. Focusing on the absorption and emission wavelengths estimated by S_0–S_1 transitions (HOMO–LUMO transitions) in the ground and excited states, respectively, it was disclosed that extension of π-conjugation reduced the Stokes shift (Figures S6 and S7). Moreover, the values of oscillator strength (f) of dimers both in absorption and emission were larger than those of monomers. Indeed, oligomers experimentally showed larger Φ_{PL}s compared to the monomers. Those behaviors also indicate extension of π-conjugation effectively occur in the TAz systems including the hypervalent bond. In contrast, calculation results suggest that other strong absorption bands around 350 nm of TAz monomers should be assigned to S_0–S_3 transitions (Table S3 and Figure S8). Interestingly, the transitions disappeared in dimers. In place of them, new two weak and slightly red-shifted absorption bands assigned to S_0–S_6 and S_0–S_7 transitions were generated, and the related MOs, HOMO−3 and HOMO−4, were not delocalized throughout the molecules unlike

HOMO. Those theoretical results can be well explained by the fact that the normalized absorbances around 350 nm of TAz derivatives gradually decreased and broadened as increasing DP (Figure 2). We previously reported that **BAz-PPV** showed very long effective conjugation length (n>50)[46]. By comparing the energy gaps of monomers, dimers, and trimers of **TAz-PPV** derivatives and **BAz-PPV**, slightly larger reduction of the energy gaps was obtained in **BAz-PPV** than that of **TAz-PPV** derivatives (Figure S9) despite large dihedral angle between two benzene rings of adjacent units. (Figure S10). Those results suggest that the monomeric units with waving conformation flexibly interact each other and the slightly bending scaffold is not disadvantage for extension of π-conjugation.

In the optimized structures in the excited state, elongation of nitrogen–nitrogen double (N=N) bond length was observed compared to those in the ground state (Figure S11). The structural relaxation should cause the large Stokes shifts and the broadened emission spectra of planar TAz derivatives. Interestingly, values of the elongation in TAz dimers were smaller than those in TAz monomers. Those results imply that the degree of structural relaxation is decreased by extension of π-conjugation. The calculation results are corresponded to the experimental data that the shapes of emission spectra of TAz derivatives were gradually sharpened as increasing DP (Figure 3).

Figure 5

3. Conclusion

We synthesized PPV-type π-conjugated polymers based on the TAz complexes having hypervalent system with the five-coordinated distorted trigonal bipyramid geometry. The maximum absorption and emission wavelengths reached NIR region over 750 nm and 810 nm, respectively, indicating that the TAz-based system can be effectively extend through π-conjugated system involving C=C and N=N bonds. The effective conjugation length was estimated to be n>10 and the value was similar to conventional PPV systems. From CV and quantum calculations, it was revealed that increasing HOMO and decreasing LUMO energy levels should be induced by the extension of π-conjugation. Furthermore, enhancing Φ_{PL} and small Stokes shift induced by polymerization were also experimentally and theoretically disclosed. We suggest that, according to the concept of "element-blocks", construction of element-supported narrow-energy-gap monomers is a new method for obtaining NIR-absorptive and emissive materials.

Acknowledgements

This work was partially supported by the Research Institute for Production Development, Japan (for M.G.) and a Grant-in-Aid for Early-Career Scientists (for M.G.) (JSPS KAKENHI Grant numbers 20K15334), for Scientific Research (B) (for K.T), (JP17H03067), for Scientific Research on Innovative Areas "New Polymeric Materials Based on Element-Blocks (No.2401)" (JP24102013) and for Challenging Research (Pioneering) (JP18H05356).

TOC

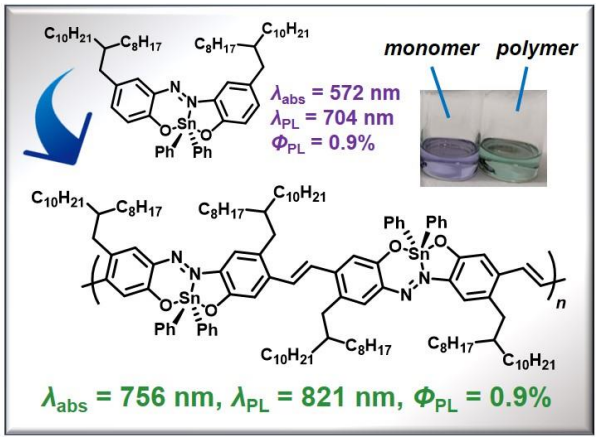
monomer
polymer
λabs = 572 nm
λPL = 704 nm
ΦPL = 0.9%
λabs = 756 nm, λPL = 821 nm, ΦPL = 0.9%

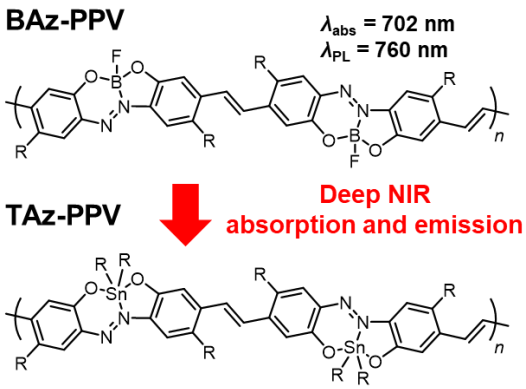

Figure 1. Chemical structures of BAz-PPV and TAz-PPV, and the concept of this research.

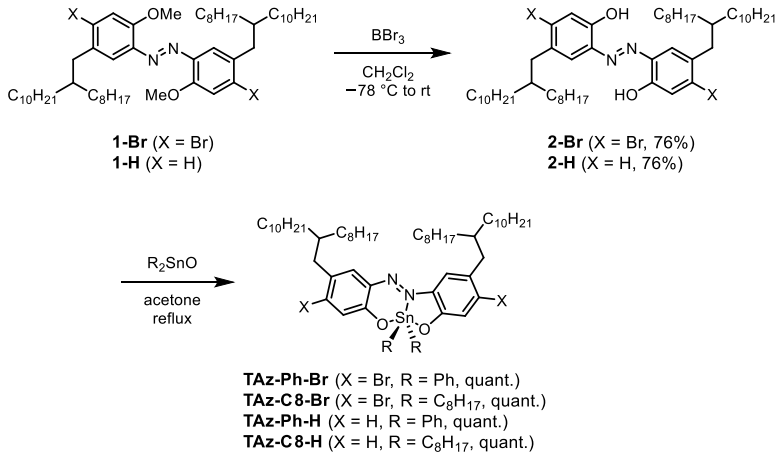

Scheme 1. Syntheses of monomers and model compounds of TAz derivatives.

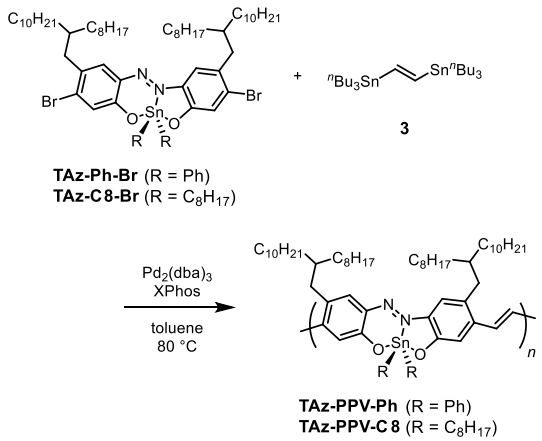

Scheme 2. Syntheses of PPV-type TAz polymers.

Table 1. Molecular dependent optical data of the TAz derivatives in solution.

	TAz-PPV-Ph						**TAz-Ph-H**
M_n /kDa [a]	41	33	19	12	8.3	6.0	1.046 [b]
n [c]	39	31	18	11	7.8	5.6	–
PDI [a]	2.2	1.7	1.5	1.5	1.4	2.0	–
λ_{abs} /nm [d]	756	756	752	749	740	730	572
λ_{PL} /nm [d]	821	818	814	814	813	812	704
ν /cm^{-1}	1047	1003	1013	1066	1213	1383	3278
Φ_{PL} /% [d,e]	0.9	1.1	1.2	1.2	1.2	1.4	0.9

	TAz-PPV-C8							**TAz-C8-H**
M_n /kDa [a]	29	16	8.8	6.2	4.2	3.2	2.2	1.118 [b]
n [c]	25	14	7.7	5.4	3.7	2.8	1.9	–
PDI [a]	1.4	1.2	1.3	1.2	1.2	1.3	1.2	–
λ_{abs} /nm [d]	752	750	744	736	723	700	667	576
λ_{PL} /nm [d]	811	807	806	801	794	789	737	700
ν /cm^{-1}	967	942	1034	1103	1237	1611	1424	3075
Φ_{PL} /% [d,e]	1.5	1.6	1.7	1.9	2.0	2.3	3.6	2.0

[a] Determined by GPC with polystyrene standards for fractionated polymers with HPLC (PDI: poly dispersity index, M_w/M_n).

[b] Molecular weights of the monomeric units, **TAz-Ph-H** and **TAz-C8-H**

[c] Degree of polymerization (M_n/M(repeating unit)).

[d] 1.0×10^{-5} M per repeating unit in chloroform, excited at an absorption maximum for PL.

[e] Absolute PL quantum yield excited at an absorption maximum.

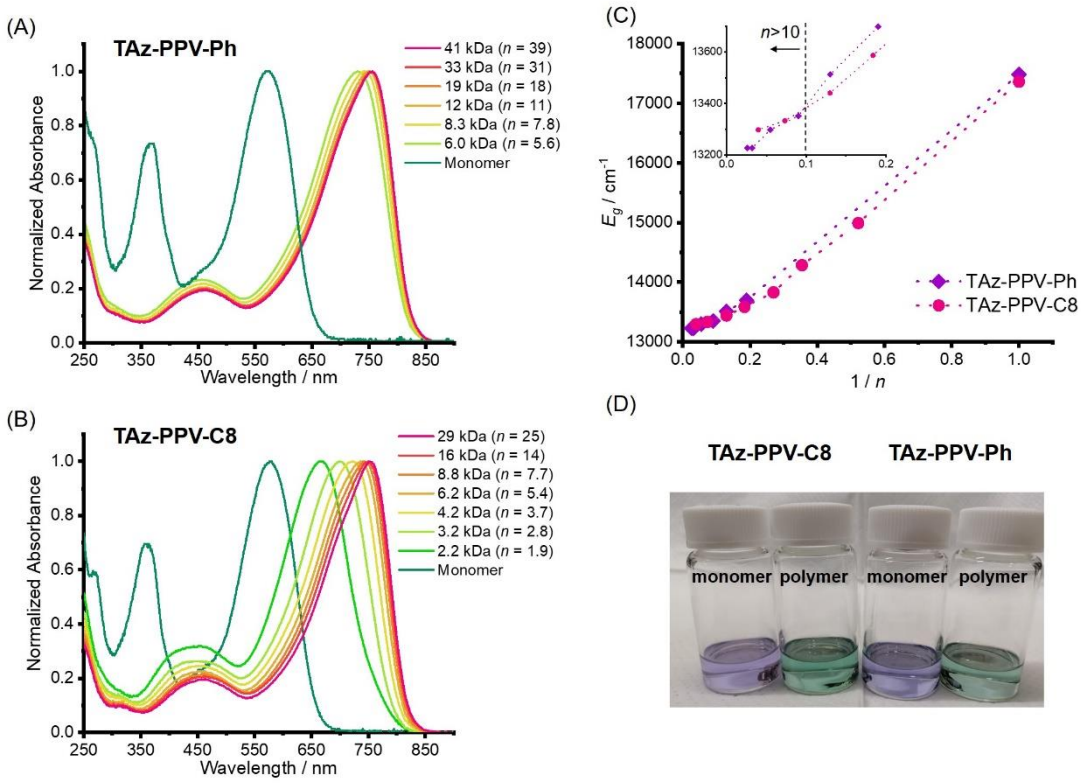

Figure 2. UV–vis absorption spectra of (A) fractionated **TAz-PPV-Ph** (polymers) and **TAz-Ph-H** (monomer) (B) fractionated **TAz-PPV-C8** (polymers) and **TAz-C8-H** (monomer) in chloroform (1.0×10^{-5} M for monomers, 1.0×10^{-5} M per repeating unit for polymers). (C) A plot of the transition energies (E_g) at maximum absorption wavelengths against $1/n$. Inserted figure denotes an enlarged plot from $1/n$ = 0.0 to 0.2. (D) Photographs of monomer (**TAz-Ph-H** and **TAz-C8-H**) and polymer (**TAz-PPV-Ph** (n=31) and **TAz-PPV-C8** (n=14)) under room light.

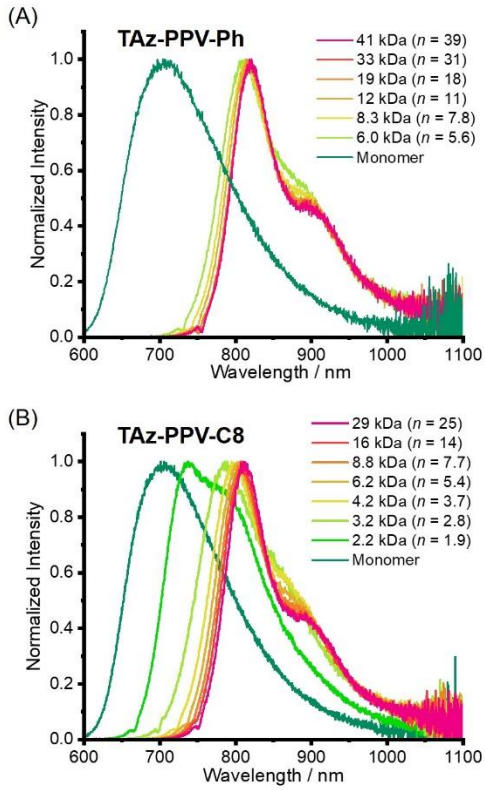

Figure 3. PL spectra of (A) fractionated **TAz-PPV-Ph** (polymers) and **TAz-Ph-H** (monomer) (B) fractionated **TAz-PPV-C8** (polymers) and **TAz-C8-H** (monomer) in chloroform (1.0×10^{-5} M for monomers, 1.0×10^{-5} M per repeating unit for polymers) with the excitation light at each absorption maximum.

Table 2. Electrochemical data of polymers and model compounds

	E_{onset}^{red} /V [a]	E_{onset}^{ox}/V [a]	E_{LUMO} [b]/eV	E_{HOMO} [b]/eV
TAz-Ph-H	−1.08	+0.62	−3.72	−5.42
TAz-PPV-Ph	−0.95	+0.41	−3.85	−5.21
TAz-C8-H	−1.20	+0.52	−3.60	−5.32
TAz-PPV-C8	−0.99	+0.35	−3.81	−5.15

[a] In CH_2Cl_2 (1.0×10^{-3} M for monomers, 1.0×10^{-3} M per repeating unit for polymers) containing $N^nBu_4PF_6$ (0.10 M) using a glassy carbon (GC) working electrode, a Pt wire counter electrode, an Ag/AgCl reference electrode, and a Fc/Fc^+ external standard at room temperature with a scan rate of 0.1 V s^{-1}.

[b] $E_{LUMO} = (-4.8-E_{onset}^{red})$ (eV), $E_{HOMO} = (-4.8-E_{onset}^{ox})$ (eV).

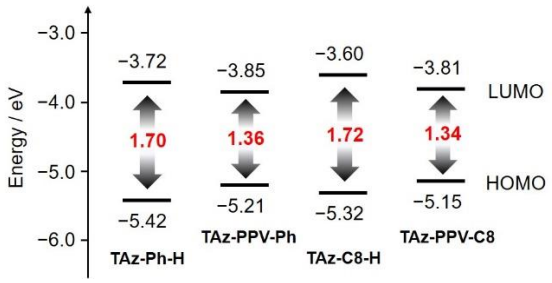

Figure 4. Energy levels and widths of energy gaps of HOMOs and LUMOs estimated from the results of cyclic voltammetry.

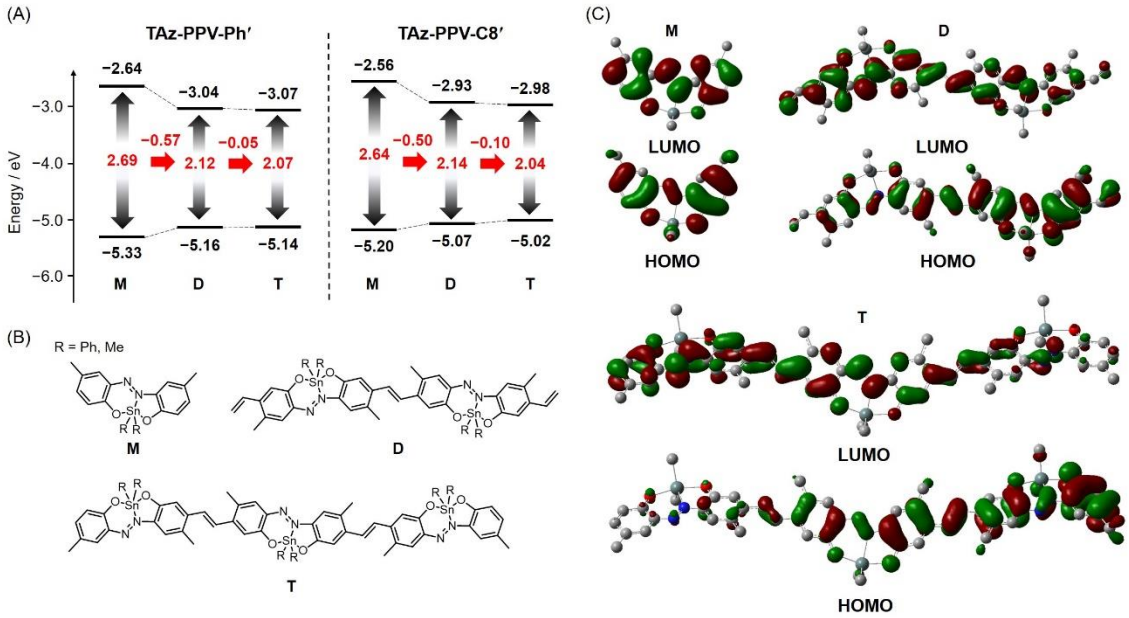

Figure 5. Results of DFT calculation at B3LYP/6-31G(d,p) for C, H, N, O and LanL2DZ for Sn levels. (A) Energy levels and energy gaps of HOMOs and LUMOs, (B) chemical structure of **TAz-PPV-Ph′** and **TAz-PPV-C8′**. (C) Kohn–Sham orbitals in monomers (M), dimers (D), and trimers (T) of **TAz-PPV-C8′**. Hydrogen atoms were omitted for clarity.

References

1. Roggo Y, Chalus P, Maurer L, Lema-Martinez C, Edmond A, Jent N. A review of near infrared spectroscopy and chemometrics in pharmaceutical technologies. J. Pharm. Biomed. Anal. 2007;44:683–700.
2. Bünzli JCG, Eliseeva SV. Lanthanide NIR luminescence for telecommunications, bioanalyses and solar energy conversion. J. Rare Earths 2010;28;824–42.
3. Cai Y, Wei Z, Song C, Tang C, Han W, Dong X. Optical nano-agents in the second near-infrared window for biomedical applications. Chem. Soc. Rev. 2019;48:22–37.
4. Ding F, Zhan Y, Lu X, Sun Y. Recent advances in near-infrared II fluorophores for multifunctional biomedical imaging. Chem. Sci. 2018;9:4370–80.
5. Ning Y, Zhu M, Zhang JL. Near-infrared (NIR) lanthanide molecular probes for bioimaging and biosensing. Coord. Chem. Rev. 2019;399:213028.
6. Li, Q, Guo Y, Liu, Y. Exploration of Near-Infrared Organic Photodetectors. Chem. Mater. 2019;31:6359–79.
7. Zou D, Zhang J, Cui Y, Qian, G. Near-infrared-emissive metal–organic frameworks. Dalton Trans. 2019;48:6669–75.
8. Huang X, Zhang W, Guan G, Song G, Zou R, Hu J. Design and Functionalization of the NIR-Responsive Photothermal Semiconductor Nanomaterials for Cancer Theranostics. Acc. Chem. Res. 2017;50:2529–38.
9. Xiang H, Cheng J, Ma X, Zhou X, Chruma JJ. Near-infrared phosphorescence: materials and applications. Chem. Soc. Rev. 2013;42:6128–85.

10. Yuan L, Lin W, Zheng K, He L, Huang W. Far-red to near infrared analyte-responsive fluorescent probes based on organic fluorophore platforms for fluorescence imaging. Chem. Soc. Rev. 2013;42:622–61.
11. Zampetti A, Minotto A, Cacialli F. Near-Infrared (NIR) Organic Light-Emitting Diodes (OLEDs): Challenges and Opportunities. Adv. Funct. Mater. 2019;29:1807623.
12. Lu H, Mack J, Yang Y, Shen Z. Structural modification strategies for the rational design of red/NIR region BODIPYs. Chem. Soc. Rev. 2014;43:4778–823.
13. Dou L, Liu Y, Hong Z, Li G, Yang Y. Low-Bandgap Near-IR Conjugated Polymers/Molecules for Organic Electronics. Chem. Rev. 2015;115:12633–65.
14. Wang Y, Zhang H, Wang Z, Feng, L. Photothermal Conjugated Polymers and Their Biological Applications in Imaging and Therapy. ACS Appl. Polym. Mater. 2020;2:4222–40.
15. Jiang Y, Pu K. Multimodal Biophotonics of Semiconducting Polymer Nanoparticles. Acc. Chem. Res. 2018;51:1840–9.
16. Kage Y, Kang S, Mori S, Mamada M, Adachi C, Kim D, Furuta H, Shimizu S. An Electron-Accepting aza-BODIPY-Based Donor–Acceptor–Donor Architecture for Bright NIR Emission. Chem. Eur. J. 2021;27:5259–67.
17. Loaeza L, Corona-Sánchez R, Castro G, Romero-Ávila M, Santillan R, Maraval V, Chauvin R, Farfán N. Synthesis and optical properties of 1-ethyl-indol-3-yl-substituted aza-BODIPY dyes at the 1,7-positions. Tetrahedron 2021;83:131983.

18. Kawano Y, Ito Y, Ito S, Tanaka K. Chujo Y. π-Conjugated Copolymers Composed of Boron Formazanate and Their Application for a Wavelength Converter to Near-Infrared Light. Macromolecules 2021;54:1934–42.
19. Sahu K, Mondal S, Mobin SM, Kar S. Photocatalytic C–H Thiocyanation of Corroles: Development of Near-Infrared (NIR)-Emissive Dyes. J. Org. Chem. 2021;86:3324–33.
20. Zhang Q, Yu P, Fan Y, Sun C, He H, Liu X, Lu L, Zhao M, Zhang H, Zhang F. Bright and Stable NIR-II J-Aggregated AIE Dibodipy-Based Fluorescent Probe for Dynamic In Vivo Bioimaging. Angew. Chem. Int. Ed. 2021;60:3967–73.
21. Grimme J, Kreyenschmidt M, Uckert F, Müllen K, Scherf U. On the conjugation length in poly(para-phenylene)-type polymers. Adv. Mater. 1995;7:292–5.
22. Rissler J. Effective conjugation length of π-conjugated systems. Chem. Phys. Lett. 2004;395:92–6.
23. Hoffmann ST, Bässler H, Köhler, A. What Determines Inhomogeneous Broadening of Electronic Transitions in Conjugated Polymers?. J. Phys. Chem. B 2010;114:17037–48.
24. Tanaka K, Chujo Y. New Idea for Narrowing an Energy Gap by Selective Perturbation of One Frontier Molecular Orbital. Chem. Lett. 2021;50:269–79.
25. Watanabe H, Tanaka K, Chujo, Y. Independently Tuned Frontier Orbital Energy Levels of 1,3,4,6,9b-Pentaazaphenalene Derivatives by the Conjugation Effect. J. Org. Chem. 2019;84:2768–78.
26. Watanabe H, Ochi J, Tanaka K. Chujo Y. Tuning the NIR Absorption Properties of 1,3,4,6,9b-Pentaazaphenalene Derivatives Through the Spatially Separated Frontier Molecular Orbitals. Eur. J. Org. Chem. 2020;777–83.

27. Watanabe H, Kawano Y, Tanaka K, Chujo, Y. Enhancing Light-Absorption and Luminescent Properties of Non-Emissive 1,3,4,6,9b-Pentaazaphenalene through Perturbation of Forbidden Electronic Transition by Boron Complexation. Asian J. Org. Chem. 2020;9:259–66.

28. Chujo Y, Tanaka K. New Polymeric Materials Based on Element-Blocks. Bull. Chem. Soc. Jpn. 2015;88:633–43.

29. Gon M, Tanaka K, Chujo Y. Recent progress in the development of advanced element-block materials. Polym. J. 2018;50:109–26.

30. Tanaka K, Chujo Y. Modulation of the solid-state luminescent properties of conjugated polymers by changing the connecting points of flexible boron element blocks. Polym. J. 2020;52:555–66.

31. Gon M, Saotome S, Tanaka K, Chujo Y. Paintable Hybrids with Thermally Stable Dual Emission Composed of Tetraphenylethene-Integrated POSS and MEH-PPV for Heat-Resistant White-Light Luminophores. ACS Appl. Mater. Interfaces 2021;13:12483–90.

32. Gon M, Sato K, Kato K, Tanaka K, Chujo Y. Preparation of bright-emissive hybrid materials based on light-harvesting POSS having radially integrated luminophores and commercial π-conjugated polymers Mater. Chem. Front. 2019;3:314–20.

33. Gon M, Kato K, Tanaka K, Chujo Y. Elastic and mechanofluorochromic hybrid films with POSS-capped polyurethane and polyfluorene. Mater. Chem. Front. 2019;3:1174–80.

34. Ochi J, Tanaka K, Chujo Y. Recent Progress in the Development of Solid-State Luminescent *o*-Carboranes with Stimuli Responsivity. Angew. Chem. Int. Ed. 2020;59:9841–55.

35. Ochi J, Tanaka K, Chujo Y. Experimental proof for emission annihilation through bond elongation at the carbon–carbon bond in *o*-carborane with fused biphenyl-substituted compounds Dalton Trans. 2021;50:1025–33.

36. Morisue M, Kusukawa T, Watase, S. Dipyrrin Complexes of Borasiloxane Silanols with Adaptive Hydrogen-Bonded Conformations in the Crystal and in Solution States. Eur. J. Inorg. Chem. 2020;1885–93.

37. Zhao R, Liu J, Wang L. Polymer Acceptors Containing B←N Units for Organic Photovoltaics. Acc. Chem. Res. 2020;53:1557–67.

38. Nishiyama H, Zheng F, Inagi S, Fueno H, Tanaka K, Tomita I. Tellurophene-containing π-conjugated polymers with unique heteroatom–heteroatom interactions by post-element-transformation of an organotitanium polymer. Polym. Chem. 2020;11:4693–8.

39. Imoto H, Naka K. The Dawn of Functional Organoarsenic Chemistry. Chem. Eur. J. 2019;25:1883–94.

40. Tanabe M, Hagio T, Osakada K, Nakamura M, Hayashi Y, Ohshita J. Synthesis of 4,4-Dihydrodithienosilole and Its Unexpected Cyclodimerization Catalyzed by Ni and Pt Complexes. Organometallics 2017;36:1974–80.

41. Gon M, Tanaka K, Chujo Y. Discovery of Functional Luminescence Properties Based on Flexible and Bendable Boron-Fused Azomethine/Azobenzene Complexes with O,N,O-Type Tridentate Ligands. Chem. Rec. doi:10.1002/tcr.202000156 (in press).

42. Ohtani S, Gon M, Tanaka K, Chujo Y. Construction of the Luminescent Donor–Acceptor Conjugated Systems Based on Boron-Fused Azomethine Acceptor. Macromolecules 2019;52:3387–93.

43. Gon M, Wakabayashi J, Nakamura M, Tanaka K, Chujo Y. Controlling Energy Gaps of π-Conjugated Polymers by Multi-Fluorinated Boron-Fused Azobenzene Acceptors for Highly Efficient Near-Infrared Emission. Chem. Asian J. 2021;16:696–703.

44. Gon M, Wakabayashi J, Nakamura M, Tanaka K, Chujo Y. Preparation of Near-Infrared Emissive π-Conjugated Polymer Films Based on Boron-Fused Azobenzene Complexes with Perpendicularly Protruded Aryl Substituents. Macromol. Rapid Commun. doi:10.1002/marc.202000566 (in press).

45. Gon M, Tanaka K, Chujo Y. A Highly Efficient Near-Infrared-Emissive Copolymer with a N=N Double-Bond π-Conjugated System Based on a Fused Azobenzene-Boron Complex. Angew. Chem. Int. Ed. 2018;57:6546–51.

46. Wakabayashi J, Gon M, Tanaka K, Chujo Y. Near-Infrared Absorptive and Emissive Poly(*p*-phenylene vinylene) Derivative Containing Azobenzene–Boron Complexes. Macromolecules 2020;53:4524–32.

47. Gon M, Wakabayashi J, Tanaka K, Chujo Y. Unique Substitution Effect at 5,5′-Positions of Fused Azobenzene–Boron Complexes with a N=N π-Conjugated System. Chem. Asian J. 2019;14:1837–43.

48. Ohtani S, Gon M, Tanaka K, Chujo Y. A Flexible, Fused, Azomethine–Boron Complex: Thermochromic Luminescence and Thermosalient Behavior in Structural Transitions between Crystalline Polymorphs. Chem. Eur. J. 2017;23:11827–33.

49. Ohtani S, Takeda Y, Gon M, Tanaka K, Chujo, Y. Facile strategy for obtaining luminescent polymorphs based on the chirality of a boron-fused azomethine complex. Chem. Commun. 2020;56:15305–8.

50. Ohtani S, Nakamura M, Gon M, Tanaka K. Chujo Y. Synthesis of fully-fused bisboron azomethine complexes and their conjugated polymers with solid-state near-infrared emission. Chem. Commun. 2020;56:6575–8.

51. Ohtani S, Gon M, Tanaka K, Chujo Y. The Design Strategy for an Aggregation- and Crystallization-Induced Emission-Active Molecule Based on the Introduction of Skeletal Distortion by Boron Complexation with a Tridentate Ligand. Crystals 2020;10:615.

52. Liu CL, Tsai FC, Chang CC, Hsieh KH, Lin JL, Chen WC. Theoretical analysis on the geometries and electronic structures of coplanar conjugated poly(azomethine)s. Polymer 2005;46:4950–7.

53. Tsuji H, Nakamura, E. Carbon-Bridged Oligo(phenylene vinylene)s: A de Novo Designed, Flat, Rigid, and Stable π-Conjugated System. Acc. Chem. Res. 2019;52:2939–49.

54. Meier H, Stalmach U, Kolshorn H. Effective conjugation length and UV/vis spectra of oligomers. Acta Polym. 1997;48:379–84.

55. Panda AN, Plasser F, Aquino AJA, Burghardt I, Lischka H. Electronically Excited States in Poly(p-phenylenevinylene): Vertical Excitations and Torsional Potentials from High-Level Ab Initio Calculations. J. Phys. Chem. A 2013;117:2181–9.

56. Cardozo TM, Aquino AJA, Barbatti M, Borges I, Lischka H. Absorption and Fluorescence Spectra of Poly(*p*-phenylenevinylene) (PPV) Oligomers: An ab Initio Simulation. J. Phys. Chem. A 2015;119:1787–95.

57. Kim DY, Grey JK, Barbara PF. A detailed single molecule spectroscopy study of the vibronic states and energy transfer pathways of the conjugated polymer MEH-PPV. Synth. Met. 2006;156:336–45.

58. Padmanaban G, Ramakrishnan, S. Fluorescence Spectroscopic Studies of Solvent- and Temperature-Induced Conformational Transition in Segmented Poly[2-methoxy-5-(2′-ethylhexyl)oxy-1,4-phenylenevinylene] (MEHPPV). J. Phys. Chem. B 2004;108:14933–41.

59. Amrutha SR, Jayakannan M. Probing the π-Stacking Induced Molecular Aggregation in π-Conjugated Polymers, Oligomers, and Their Blends of *p*-Phenylenevinylenes. J. Phys. Chem. B 2008;112:1119–29.

60. Blayney AJ, Perepichka IF, Wudl F, Perepichka DF. Advances and Challenges in the Synthesis of Poly(p-phenylene vinylene)-Based Polymers. Isr. J. Chem. 2014;54:674–88.

61. Greenham NC, Moratti SC, Bradley DDC, Friend RH, Holmes AB. Efficient light-emitting diodes based on polymers with high electron affinities. Nature 1993;365:628–30.

62. Lei T, Dou JH, Cao XY, Wang JY, Pei J. Electron-Deficient Poly(*p*-phenylene vinylene) Provides Electron Mobility over 1 cm^2 V^{-1} s^{-1} under Ambient Conditions. J. Am. Chem. Soc. 2013;135:12168–71.

63. Savagatrup S, Printz AD, O'Connor TF, Zaretski AV. Lipomi DJ. Molecularly Stretchable Electronics. Chem. Mater. 2014;26:3028–41.

64. Gon M, Tanaka K, Chujo Y. Vapochromic Luminescent π-Conjugated Systems with Reversible Coordination-Number Control of Hypervalent Tin(IV)-Fused Azobenzene Complexes. Chem. Eur. J. doi:10.1002/chem.202100571 (in press).

65. Bessler KE, dos Santos JA, Deflon VM, de Souza Lemos S, Niquet E. Organotin Dyes: Synthesis and Structural Characterization of Dibutyltin and Dimethyltin Complexes with 2, 2′-Dihydroxyazobenzene. Z. anorg. allg. Chem. 2004;630:742–5.

66. Kosugi M, Sasazawa K, Shimizu Y, Migita T. REACTIONS OF ALLYLTIN COMPOUNDS III. ALLYLATION OF AROMATIC HALIDES WITH ALLYLTRIBUTYLTIN IN THE PRESENCE OF TETRAKIS(TRIPHENYLPHOSPHINE)PALLADIUM(O). Chem. Lett. 1977;6:301–2.

67. Milstein D, Stille JK. A general, selective, and facile method for ketone synthesis from acid chlorides and organotin compounds catalyzed by palladium. J. Am. Chem. Soc. 1978;100:3636–8.

68. Englman R, Jortner J. The energy gap law for radiationless transitions in large molecules. Mol. Phys. 1970;18:145–64.

69. Chynwat V, Frank HA. The application of the energy gap law to the S1 energies and dynamics of carotenoids. Chem. Phys. 1995;194:237–44.

70. Biczók L, Bérces T, Inoue H. Effects of Molecular Structure and Hydrogen Bonding on the Radiationless Deactivation of Singlet Excited Fluorenone Derivatives. J. Phys. Chem. A 1999;103:3837–42.

71. Yeo H, Tanaka K, Chujo Y. Tunable Optical Property between Pure Red Luminescence and Dual Emission Depended on the Length of Light-Harvesting Antennae in the Dyads Containing the Cardo Structure of BODIPY and Oligofluorene. Macromolecules 2016;49:8899–904.

72. Pommerehne J, Vestweber H, Guss W, Mahrt RF, Bässler H, Porsch M, Daub J. Efficient two layer leds on a polymer blend basis. Adv. Mater. 1995;7:551–4.

73. Cardona CM, Li W, Kaifer AE, Stockdale D, Bazan GC. Electrochemical Considerations for Determining Absolute Frontier Orbital Energy Levels of Conjugated Polymers for Solar Cell Applications. Adv. Mater. 2011;23:2367–71.

74. Meyers F, Heeger AJ, Brédas JL. Fine tuning of the band gap in conjugated polymers via control of block copolymer sequences. J. Chem. Phys. 1992;97:2750–8.

75. Ma J, Li S, Jiang Y. A Time-Dependent DFT Study on Band Gaps and Effective Conjugation Lengths of Polyacetylene, Polyphenylene, Polypentafulvene, Polycyclopentadiene, Polypyrrole, Polyfuran, Polysilole, Polyphosphole, and Polythiophene. Macromolecules 2002;35:1109–15.

Supplementary Information

PPV-Type π-Conjugated Polymers Based on Hypervalent Tin(IV)-fused Azobenzene Complexes Showing Near-Infrared Absorption and Emission

Masayuki Gon, Kazuya Tanimura, Misao Yaegashi, Kazuo Tanaka and Yoshiki Chujo*

Department of Polymer Chemistry, Graduate School of Engineering, Kyoto University Katsura, Nishikyo-ku, Kyoto 615-8510, Japan

E-mail: tanaka@poly.synchem.kyoto-u.ac.jp

Contents page

General

^{1}H, $^{13}C\{^{1}H\}$ and ^{119}Sn NMR spectra were recorded on JEOL AL400 and ECX400 instruments at 400, 100 and 149 MHz, respectively. Samples were analyzed in $CDCl_3$. The chemical shift values were expressed relative to Me_4Si for ^{1}H, $^{13}C\{^{1}H\}$ NMR as an internal standard in $CDCl_3$ and Me_4Sn for ^{119}Sn NMR as a capillary standard. Analytical thin layer chromatography (TLC) was performed with silica gel 60 Merck F254 plates. Column chromatography was performed with Wakogel® C-300 silica gel. High-resolution mass (HRMS) spectrometry was performed at the Technical Support Office (Department of Synthetic Chemistry and Biological Chemistry, Graduate School of Engineering, Kyoto University), and the HRMS spectra were obtained on a Thermo Fisher Scientific EXACTIVE spectrometer for electrospray ionization (ESI) and a Thermo Fisher Scientific EXACTIVE spectrometer for atmospheric pressure chemical ionization (APCI). UV–vis–NIR spectra were recorded on a SHIMADZU UV-3600 spectrophotometer, and samples were analyzed at room temperature. Fluorescence emission spectra were measured with a HORIBA Duetta spectrofluorometer at room temperature. Absolute photoluminescence quantum yield (Φ_{PL}) was recorded on a Hamamatsu Photonics Quantaurus-QY Plus C13534-01 at room temperature. Gel permeation chromatography (GPC) was carried out on a TOSOH G3000HXI system equipped with three consecutive polystyrene gel columns (TOSOH gels: α-4000, α-3000, α-2500) using chloroform as an eluent after calibration with standard polystyrene samples (1.0 mL/min) at 40 ºC. Recyclable preparative high-performance liquid chromatography (HPLC) was carried out on a Japan Analytical Industry Model LC-9204 (JAIGEL-2.5H and 3HH columns) using $CHCl_3$ as an eluent at room temperature.

Materials

Commercially available compounds used without purification:

Boron tribromide (17% in CH_2Cl_2, ca. 1 M) (BBr_3 in CH_2Cl_2) (Tokyo Chemical Industry Co, Ltd.)

Diphenyltin(IV) oxide (Sigma-Aldrich Co. LLC.)

Dioctyltin(IV) oxide (FUJIFILM Wako Pure Chemical Industries, Ltd.)

trans-1,2-Bis(tributylstannyl)ethylene (Tokyo Chemical Industry Co, Ltd.)

$Pd_2(dba)_3$ (dba = dibenzylideneacetone) (Tokyo Chemical Industry Co, Ltd.)

2-Dicyclohexylphosphino-2′,4′,6′-triisopropylbiphenyl (XPhos) (Strem Chemicals, Inc.)

Commercially available solvents:

MeOH (FUJIFILM Wako Pure Chemical Industries, Ltd.), toluene (deoxidized grade, FUJIFILM Wako Pure Chemical Industries, Ltd.) CH_2Cl_2 (deoxidized grade, FUJIFILM Wako Pure Chemical Industries, Ltd.) used without purification.

Compounds prepared as described in the literatures:

Compound **1-Br** [1]

Compound **1-H** [1]

Synthetic procedures and characterization

Synthesis of Monomers

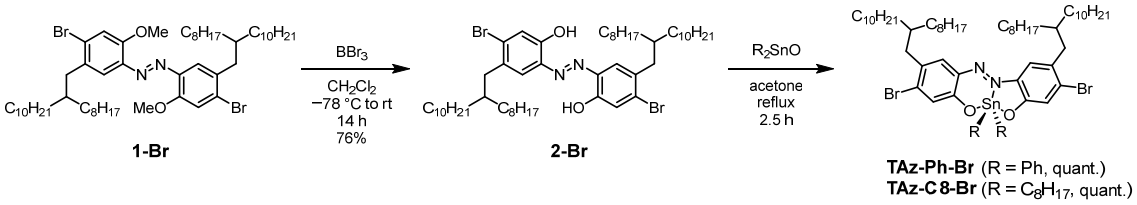

Synthesis of **2-Br**

1-Br (0.400 g, 0.416 mmol, 1 equiv.) was placed in a round-bottom flask equipped with a magnetic stirring bar. After degassing and filling N_2 three times, CH_2Cl_2 (10 mL) was added to the flask. After cooling the mixture to −78 °C, BBr_3 (1 M in CH_2Cl_2, 2.08 mL, 2.08 mmol, 5.12 equiv.) was dropwise added. The reaction was carried out at room temperature for 14 h. After the reaction, MeOH was carefully added at 0 °C for quenching the reaction and the solvent was removed with a rotary evaporator. The residue was purified by column chromatography on SiO_2 (hexane/CH_2Cl_2 = 3/1 v/v as an eluent) to afford **2-Br** (0.297 g, 0.318 mmol, 76%) as an orange oil.

R_f = 0.75 (hexane/CH_2Cl_2 = 3/1 v/v). ^{1}H NMR ($CHCl_3$, 400 MHz) δ 12.02 (s, 2H), 7.45 (s, 2H), 7.27 (s, 2H), 2.65 (d, J = 7.2 Hz, 4H), 1.75 (s, 2H), 1.28–1.24 (br, 64H), 0.89–0.84 (br, 12H) ppm; ^{13}C{^{1}H} NMR ($CDCl_3$, 100 MHz) δ 151.0, 134.3, 133.5, 132.5, 130.1, 122.6, 40.0, 37.9, 33.2, 31.9, 31.9, 30.0, 29.7, 29.6, 29.6, 29.3, 29.3, 26.5, 22.7, 22.7, 14.1 ppm; HRMS (ESI) calcd. for $C_{52}H_{89}Br_2N_2O_2$ $[M+H]^+$: 931.5285, found: 931.5273.

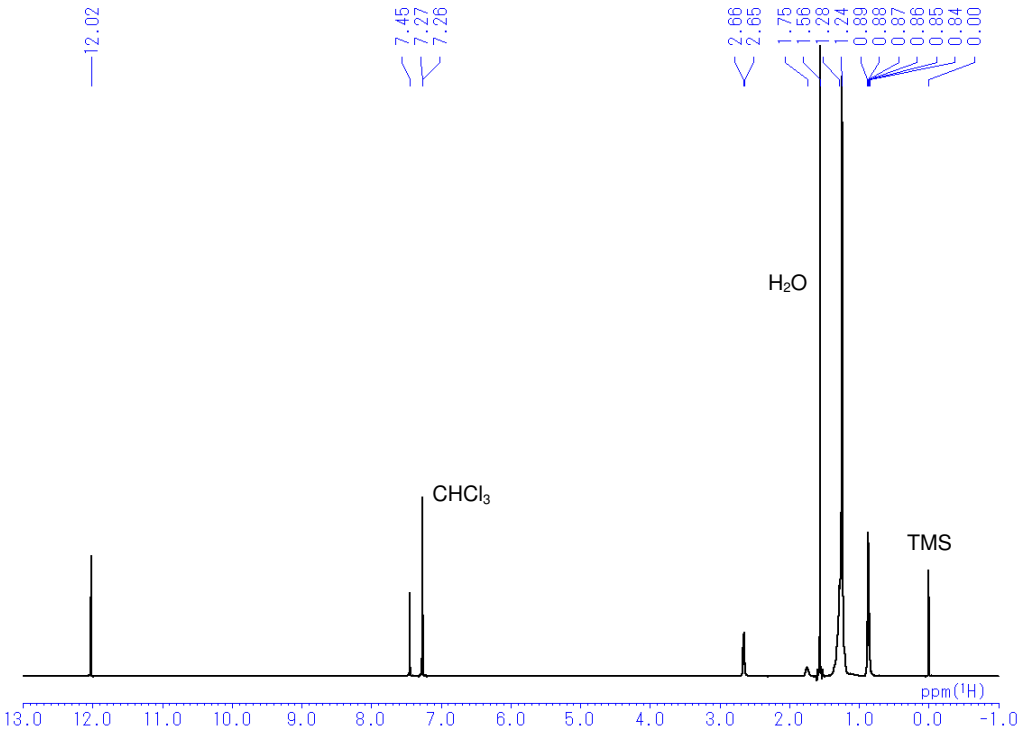

Chart S1. ^{1}H NMR spectrum of **2-Br** in $CDCl_3$.

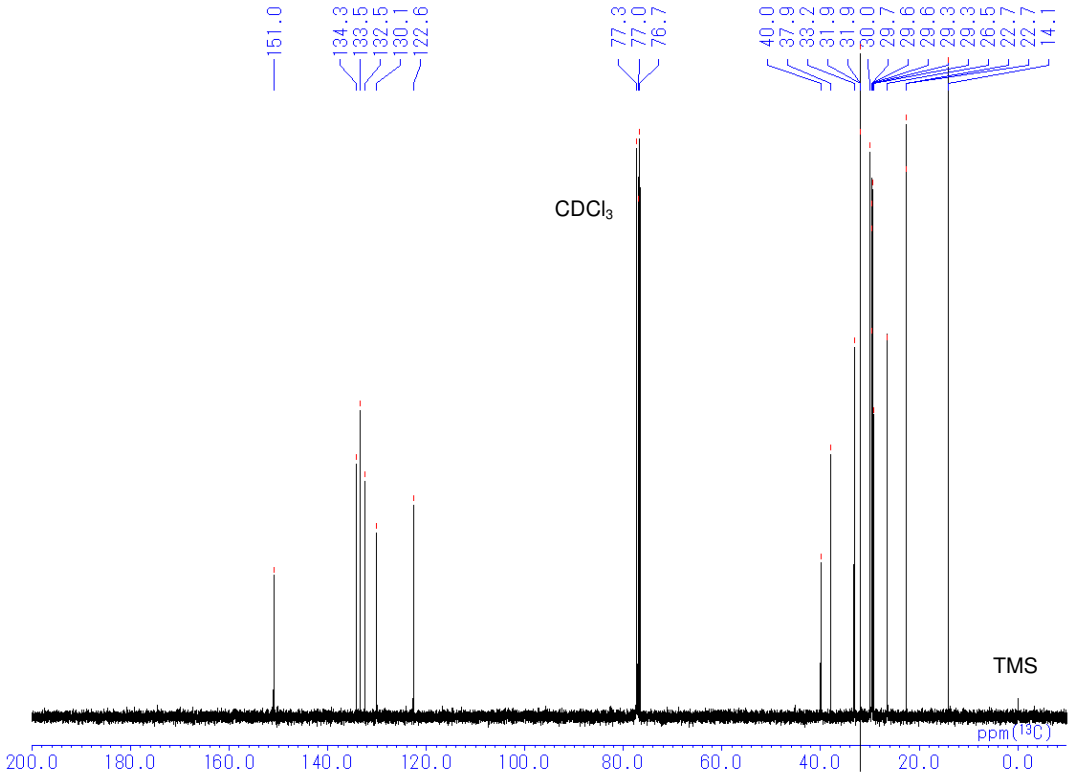

Chart S2. ^{13}C{^{1}H} NMR spectrum of **2-Br** in $CDCl_3$.

Synthesis of **TAz-Ph-Br**

In a 20 mL round bottom flask, **2-Br** (0.100 g, 0.107 mmol, 1 equiv.), diphenyltin(IV) oxide (0.0464 g, 0.161 mmol, 1.5 equiv.) and acetone (5 mL) were added under N_2. Then, the solution was stirred at reflux temperature for 2.5 h. Insoluble products were filtered, and the solution was concentrated *in vacuo* to give **TAz-Ph-Br** (0.135 g, 0.107 mmol, quant.) as a violet oil.

^{1}H NMR ($CHCl_3$, 400 MHz) δ 7.87–7.84 (m, 2H), 7.44–7.33 (m, 8H), 7.85 (s, 1H), 7.48 (s, 1H), 7.35 (s, 1H), 7.33(s, 1H), 2.61–2.57 (m, 4H), 1.73 (m, 2H), 1.27–1.23 (br, 64H), 0.88–0.83 (br, 12H) ppm; ^{13}C{^{1}H} NMR ($CDCl_3$, 100 MHz) δ 160.0, 158.5, 138.8, 136.7, 136.3, 136.1, 136.0, 135.1, 132.1, 131.6, 131.1, 130.7, 129.0, 127.2, 124.0, 118.1, 40.2, 39.8, 37.8, 37.8, 33.2, 33.0, 33.0, 31.9, 31.9, 30.0, 30.0, 29.7, 29.7, 29.7, 29.4, 29.3, 26.5, 26.5, 26.4, 22.7, 22.7, 22.7, 14.1, 14.1 ppm; ^{119}Sn NMR ($CDCl_3$, 149 MHz) δ −363.3 ppm. HRMS (ESI) calcd. for $C_{64}H_{96}Br_2ClN_2O_2Sn$ $[M+Cl]^+$: 1237.4528, found: 1237.4546.

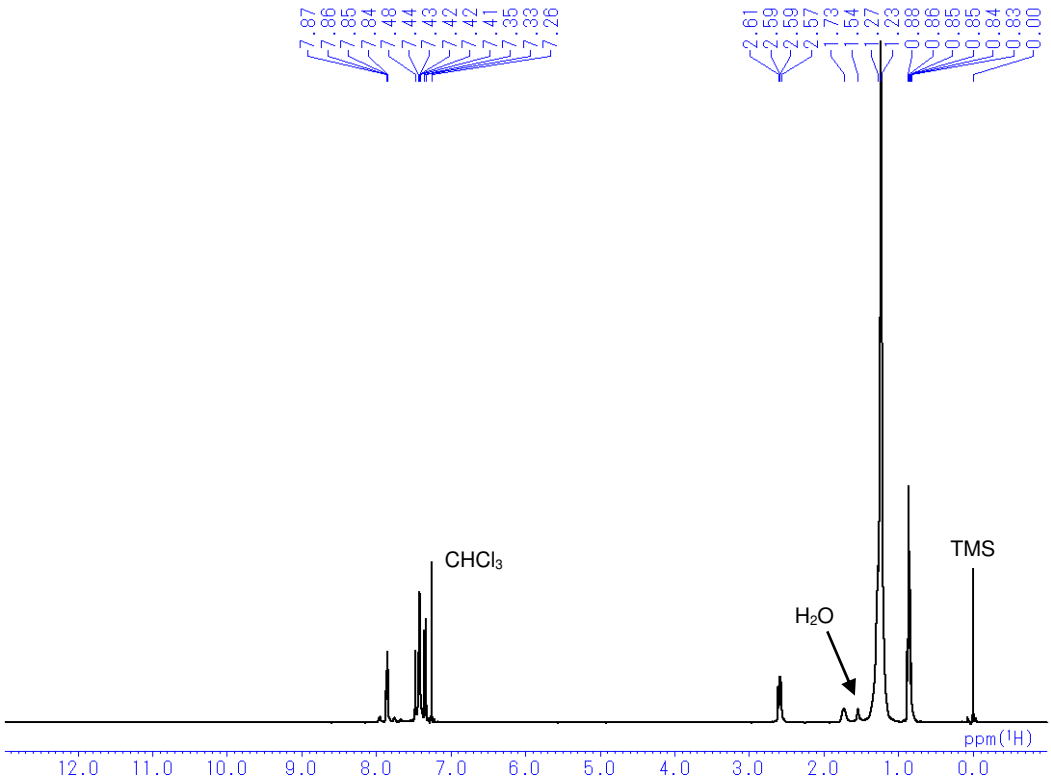

Chart S3. ^{1}H NMR spectrum of **TAz-Ph-Br** in $CDCl_3$.

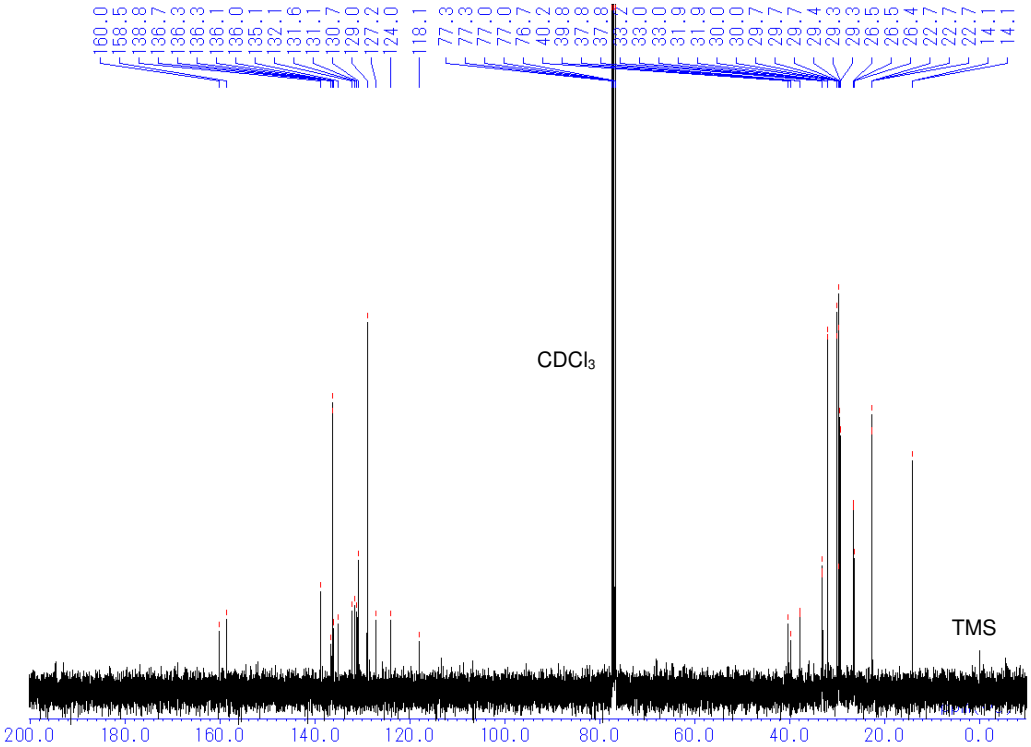

Chart S4. $^{13}C\{^{1}H\}$ NMR spectrum of **TAz-Ph-Br** in $CDCl_3$.

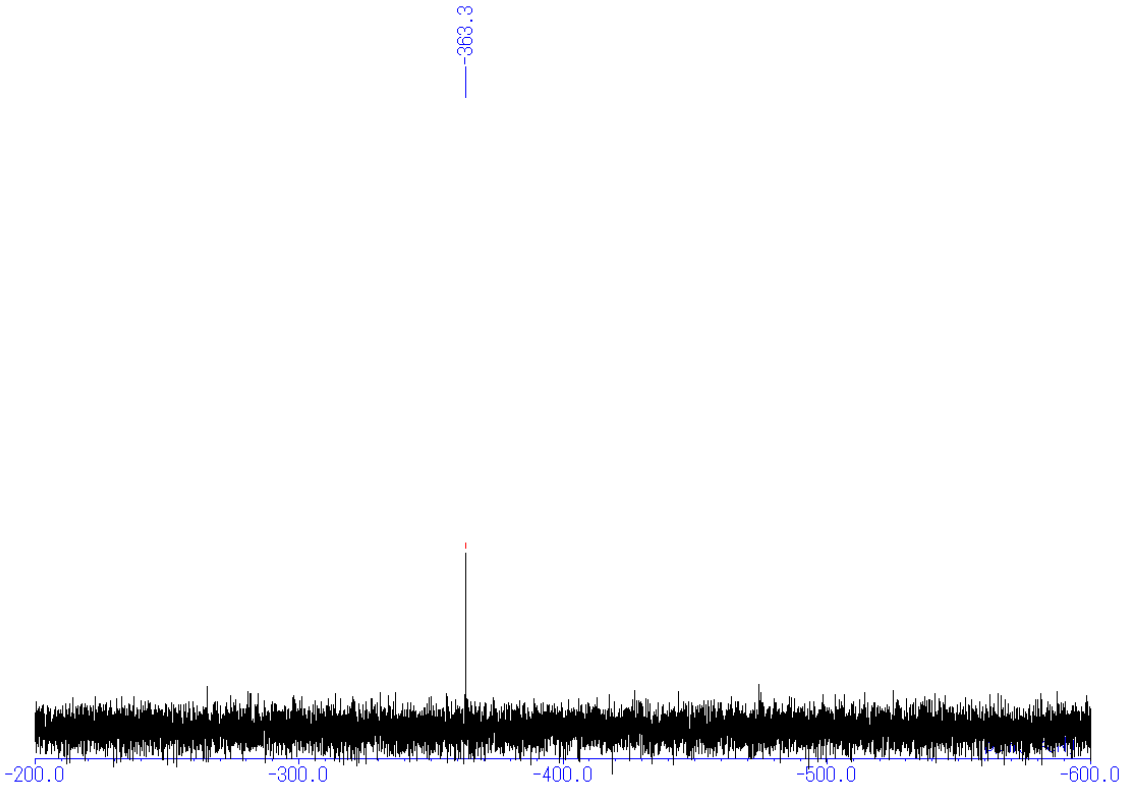

Chart S5. ^{119}Sn NMR spectrum of **TAz-Ph-Br** in $CDCl_3$.

Synthesis of **TAz-C8-Br**

In a 20 mL round bottom flask, **2-Br** (0.296 g, 0.317 mmol, 1 equiv.), dioctyltin(IV) oxide (0.172 g, 0.476 mmol, 1.5 equiv.) and acetone (5 mL) were added under N_2. Then, the solution was stirred at reflux temperature for 2.5 h. Insoluble products were filtered, and the solution was concentrated *in vacuo* to give **TAz-C8-Br** (0.405 g, 0.317 mmol, quant.) as a violet oil.

^{1}H NMR ($CHCl_3$, 400 MHz) δ 7.47 (s, 1H), 7.30 (s, 1H), 7.07 (s, 1H), 7.03 (s, 1H), 2.60–2.58 (m, 4H), 1.74 (m, 2H), 1.66–1.61 (m, 4H), 1.54–1.48 (br, 2H), 1.25–1.19 (br, 86H), 0.89–0.84 (m, 18H) ppm; ^{13}C{^{1}H} NMR ($CDCl_3$, 100 MHz) δ 160.6, 158.4, 136.8, 135.7, 134.5, 131.8, 130.9, 127.0, 123.7, 118.0, 40.2, 37.8, 37.8, 33.5, 33.2, 33.1, 31.9, 31.8, 30.1, 30.1, 29.7, 29.7, 29.7, 29.7, 29.6, 29.4, 29.3, 29.1, 29.0, 26.5, 26.4, 26.4, 24.7, 23.3, 23.3, 22.7, 22.7, 22.6, 14.1, 14.1 ppm; ^{119}Sn NMR ($CDCl_3$, 149 MHz) δ −217.5 ppm. HRMS (ESI) calcd. for $C_{68}H_{120}Br_2ClN_2O_2Sn$ $[M+Cl]^+$: 1309.6406, found: 1309.6428.

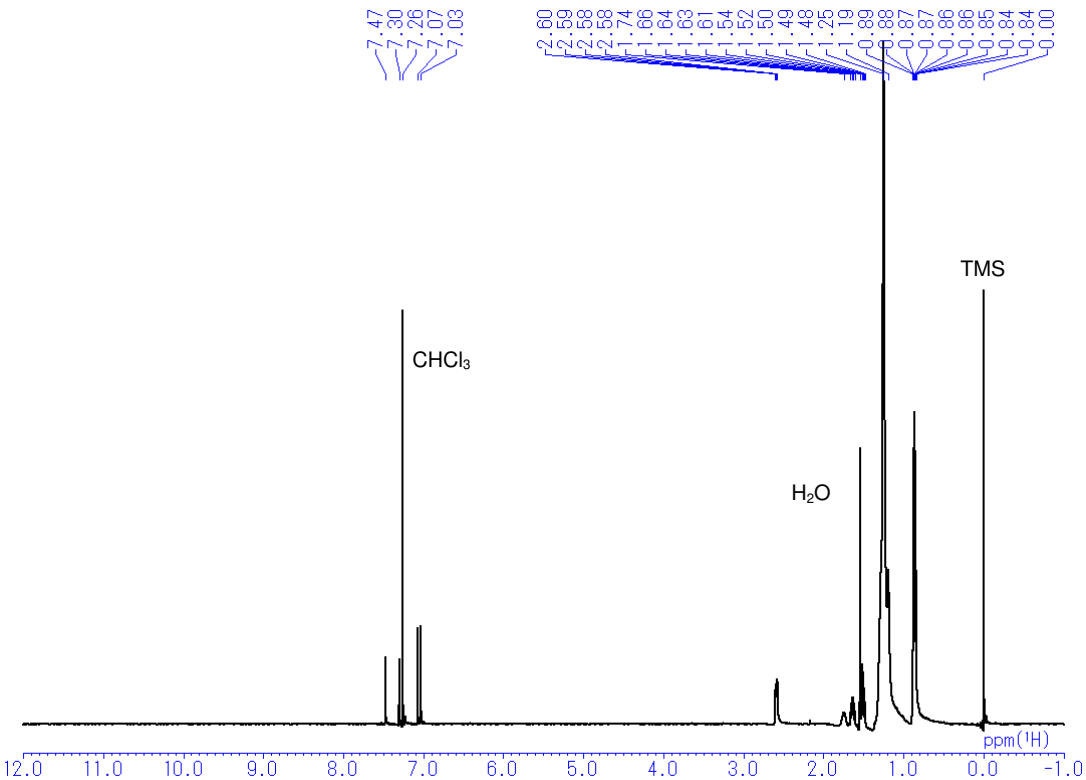

Chart S6. ^{1}H NMR spectrum of **TAz-C8-Br** in $CDCl_3$.

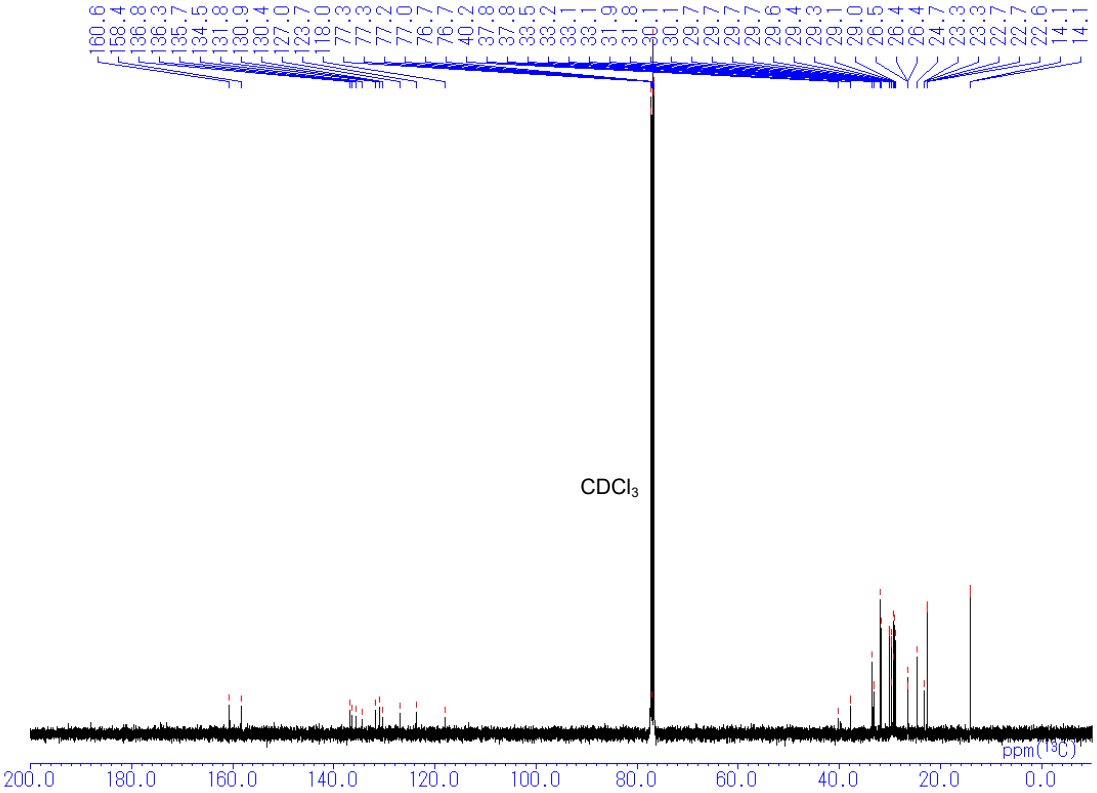

Chart S7. $^{13}C\{^{1}H\}$ NMR spectrum of **TAz-C8-Br** in $CDCl_3$.

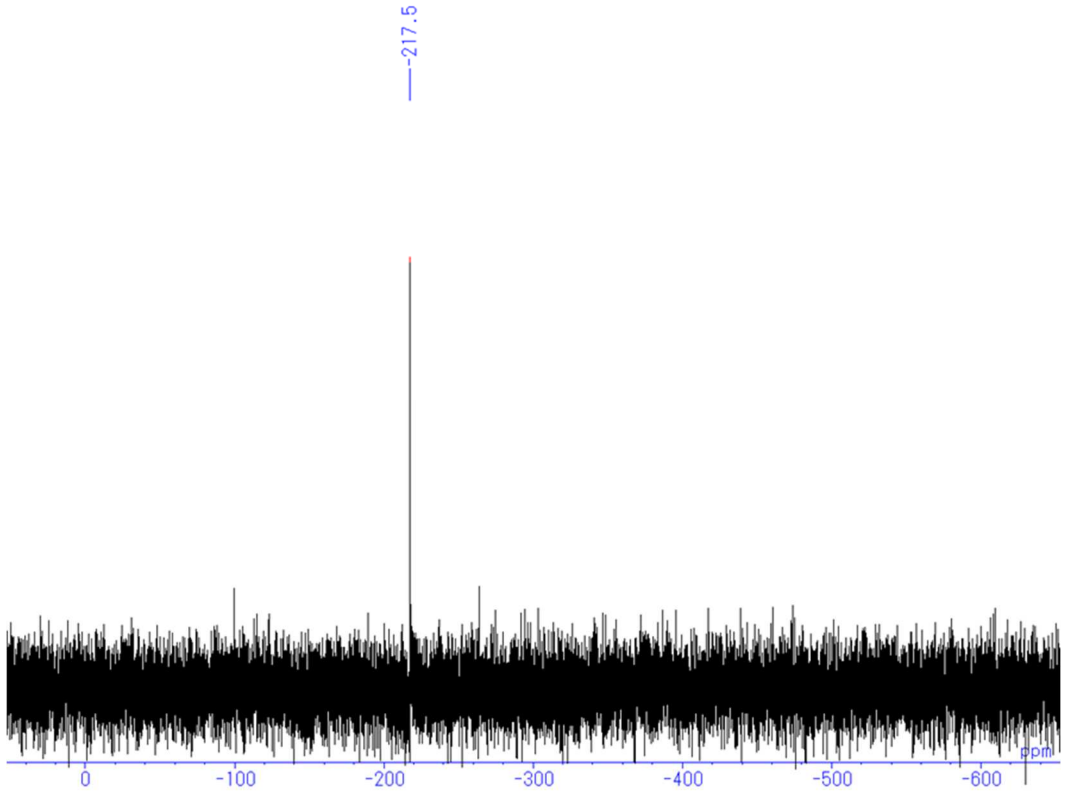

Chart S8. ^{119}Sn NMR spectrum of **TAz-C8-Br** in $CDCl_3$.

Synthesis of Polymers

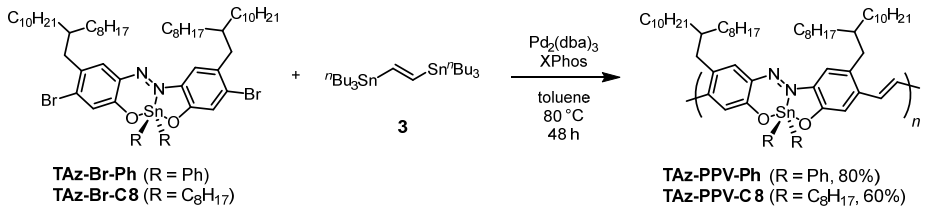

Synthesis of **TAz-PPV-Ph**

In a Schlenk tube, **TAz-Ph-Br** (0.0830 g, 0.0883 mmol, 1 equiv.), $Pd_2(dba)_3$ (0.00243 g, 0.0265 mmol, 0.03 equiv.), XPhos (0.00253 g, 0.00530 mmol, 0.06 equiv.) were added. Then, under N_2, (*E*)-1,2-bis(tributylstannyl)ethene (0.0535 g, 0.0883 mmol, 1 equiv.) and 2.5 mL of toluene were added and stirred at 80 °C for 48 h. Reprecipitation from $CHCl_3/CH_3CN$ gave **TAz-PPV-Ph** as a dark greenish solid (0.0856 g, 80%).

M_n = 9,500, M_w = 30,300 M_w/M_n = 3.2. ^{1}H NMR ($CDCl_3$, 400 MHz) δ 7.54, 7.31, 7.30, 7.23, 7.22, 7.11, 7.03 ppm; $^{13}C\{^1H\}$ NMR ($CDCl_3$, 100 MHz) δ 32.0, 31.9, 30.2, 29.8, 29.5, 29.2, 29.1, 22.7, 22.7, 14.1 ppm. ^{119}Sn NMR signal was not detected propbably because of broadening peaks in a polymer. In place of ^{119}Sn NMR, we confirmed the preservation of tin atom after polymerization by detecion of repeating units from a MALDI-TOF MS measurement (negative, matrix: *trans*-2-[3-(4-*tert*-Butylphenyl)-2-methyl- 2-propenylidene]malononitrile (DCTB)).

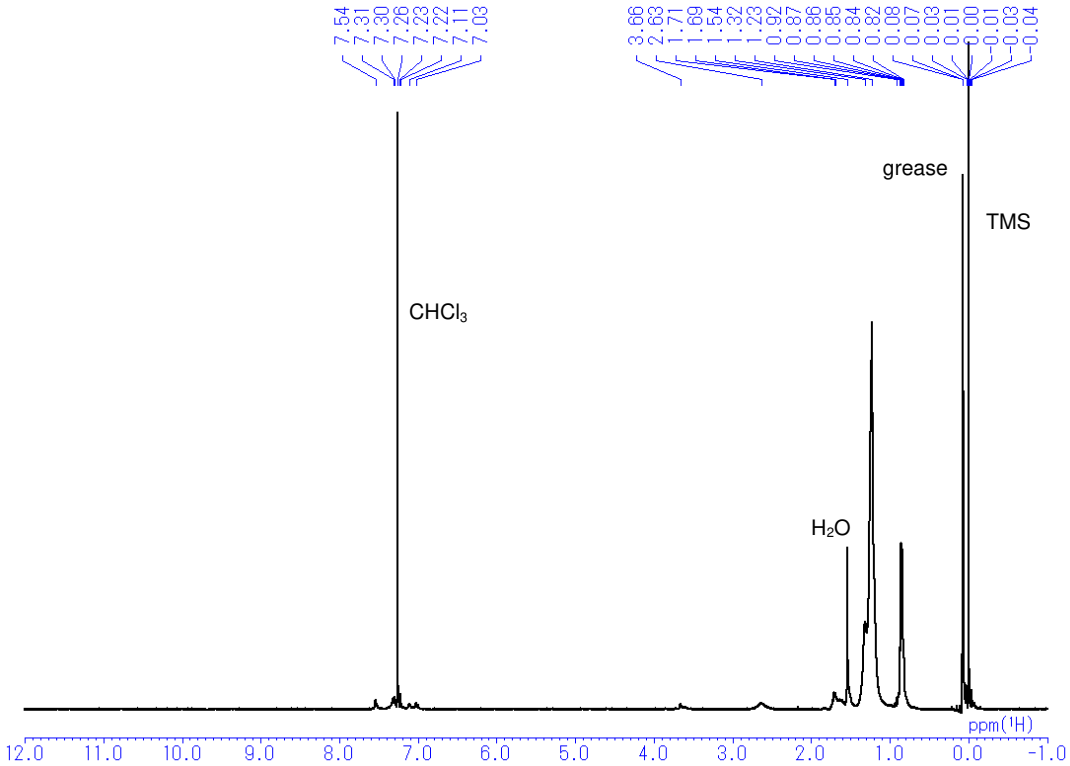

Chart S9. ^{1}H NMR spectrum of **TAz-PPV-Ph** in $CDCl_3$.

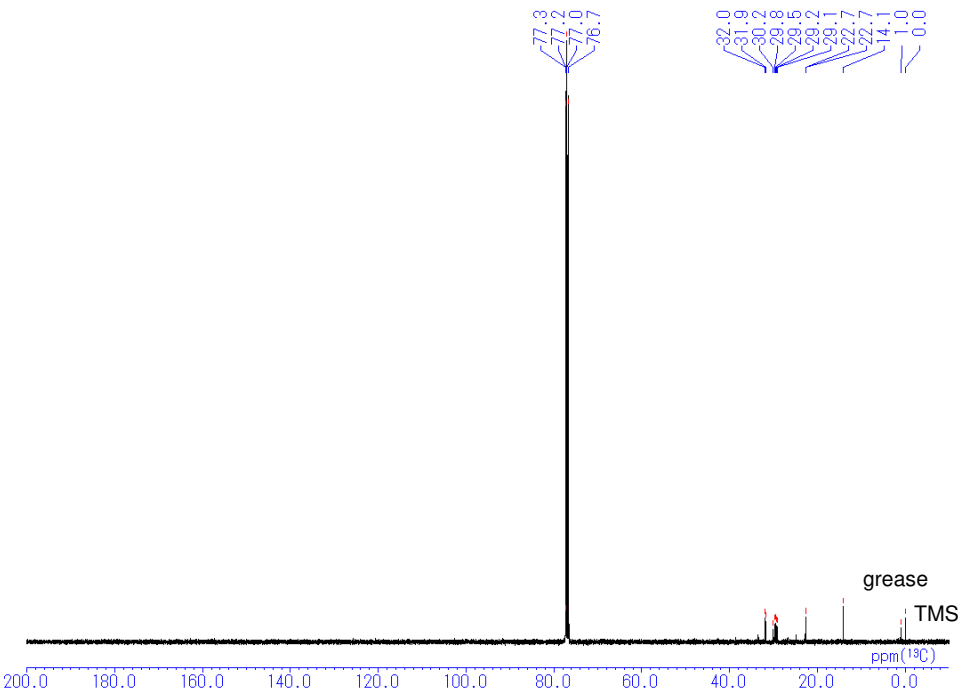

Chart S10. ^{13}C{^{1}H} NMR spectrum of **TAz-PPV-Ph** in $CDCl_3$.

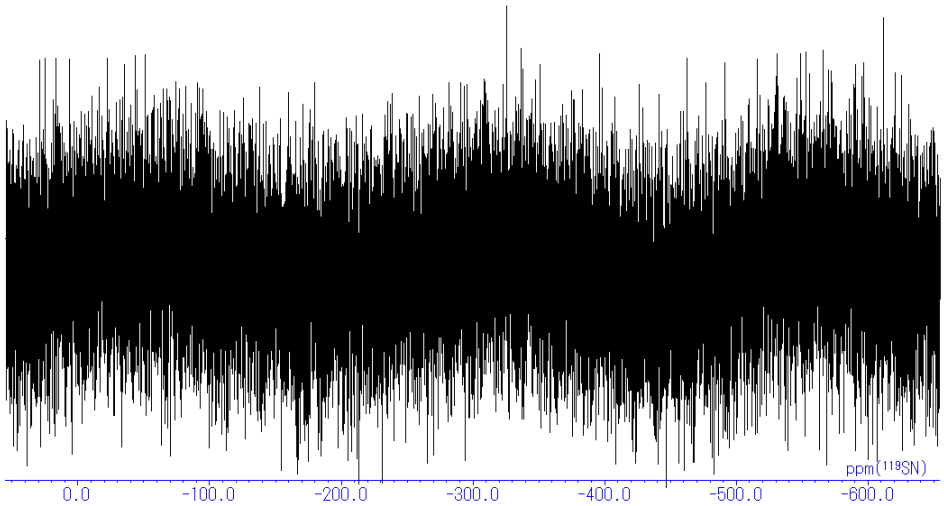

Chart S11. ^{119}Sn NMR spectrum of **TAz-PPV-Ph** in $CDCl_3$.

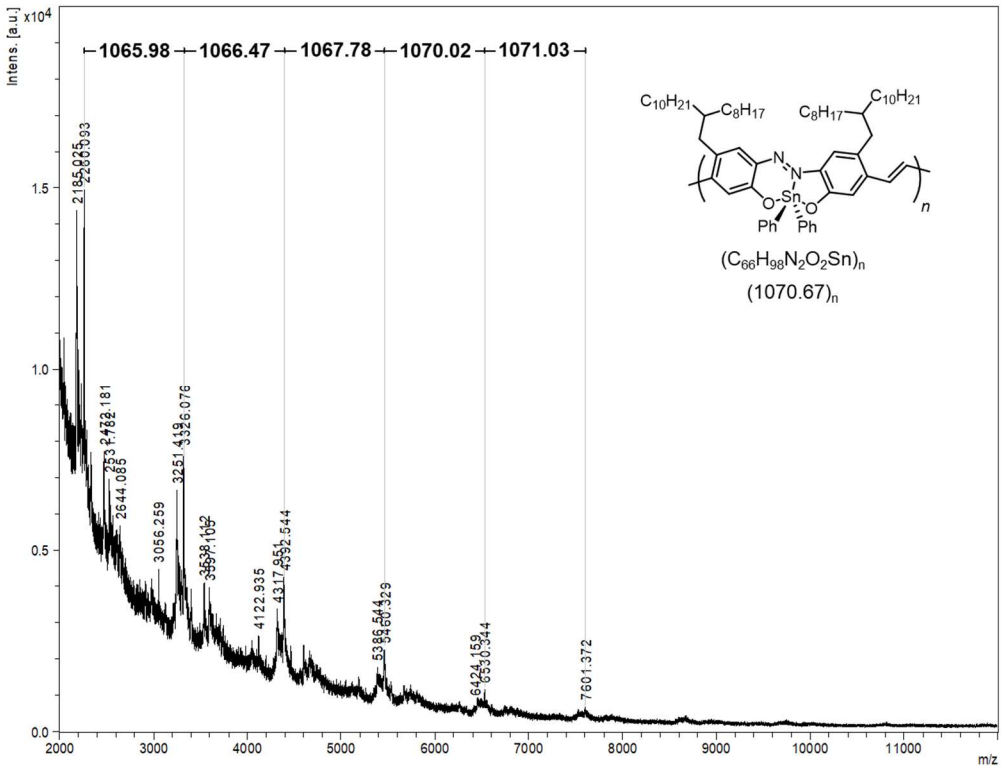

Chart S12. MADLI-TOF MS spectrum of **TAz-PPV-Ph**.

Synthesis of **TAz-PPV-C8**

In a Schlenk tube, **TAz-C8-Br** (0.0830 g, 0.0883 mmol, 1 equiv.), $Pd_2(dba)_3$ (0.00243 g, 0.0265 mmol, 0.03 equiv.), XPhos (0.00253 g, 0.00530 mmol, 0.06 equiv.) were added. Then, under N_2, (*E*)-1,2-bis(tributylstannyl)ethene (0.0535 g, 0.0883 mmol, 1 equiv.) and 2.5 mL of toluene were added and stirred at 80 °C for 48 h. Reprecipitation from $CHCl_3/CH_3CN$ gave **TAz-PPV-C8** as a dark greenish solid (0.0685 g, 60%).

M_n = 4,600, M_w = 11,000, M_w/M_n = 2.4. ^{1}H NMR ($CDCl_3$, 400 MHz) δ 7.97, 7.52, 7.42, 7.29, 7.23, 7.22, 1.36, 1.25, 1.18, 1.14, 0.83, 0.81, 0.78 ppm; $^{13}C\{^1H\}$ NMR ($CDCl_3$, 100 MHz) δ 31.9, 30.2, 29.7, 29.4, 22.7, 14.1 ppm. ^{119}Sn NMR signal was not detected propbably because of broadening peaks in a polymer. In place of ^{119}Sn NMR, we confirmed the preservation of tin atom after polymerization by detecion of repeating units from a MALDI-TOF MS measurement (negative, matrix: *trans*-2-[3-(4-*tert*-Butylphenyl)-2-methyl-2-propenylidene]malononitrile (DCTB)). The different molecular weight of two main peaks was ca. 290 Da and that was asigned to a terminal unit of Sn^nBu_3 (calcd. for $C_{12}H_{27}Sn$: 290.16).

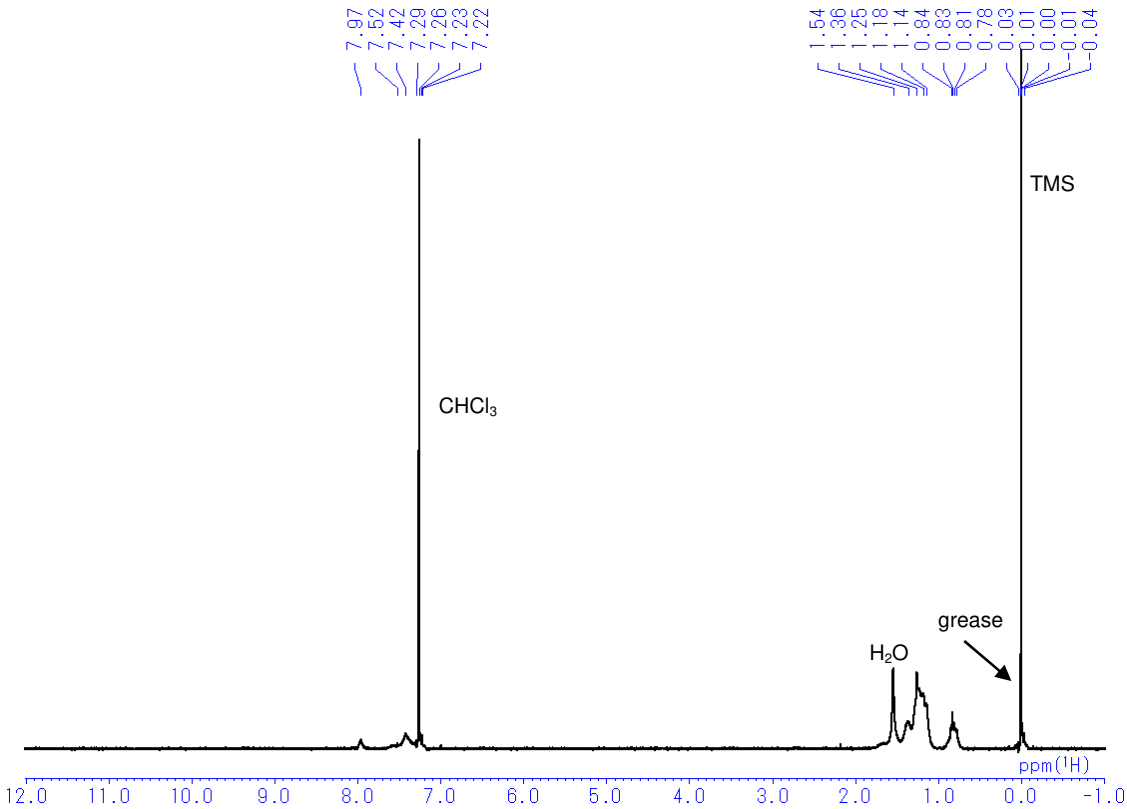

Chart S13. ^{1}H NMR spectrum of **TAz-PPV-C8** in $CDCl_3$.

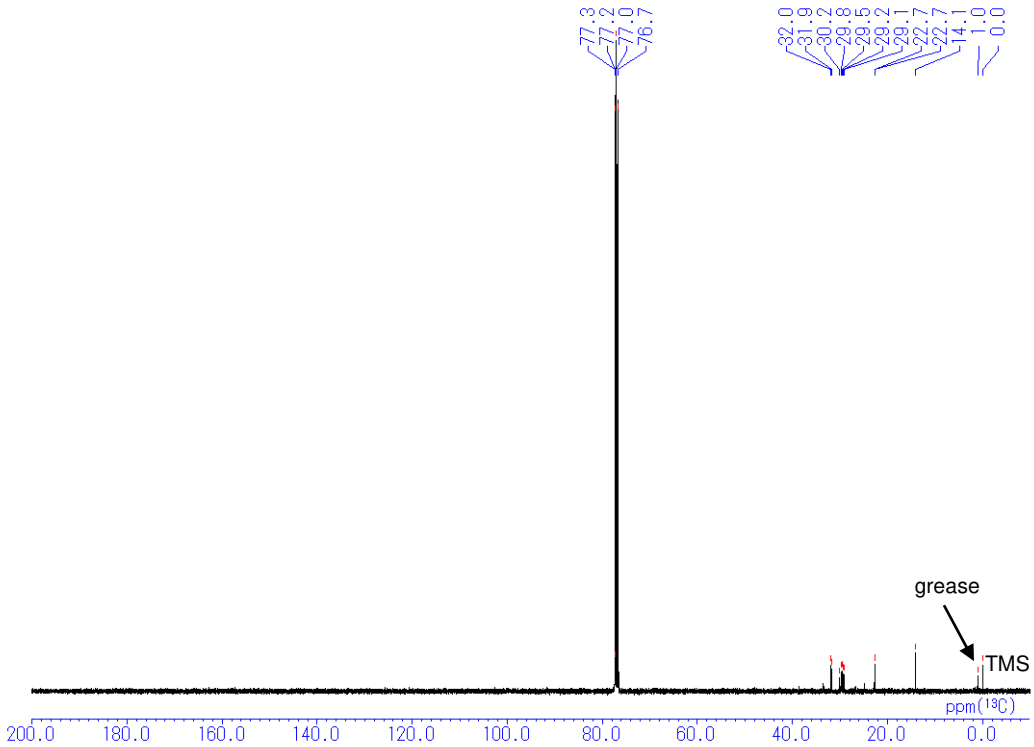

Chart S14. ^{13}C{^{1}H} NMR spectrum of **TAz-PPV-C8** in $CDCl_3$.

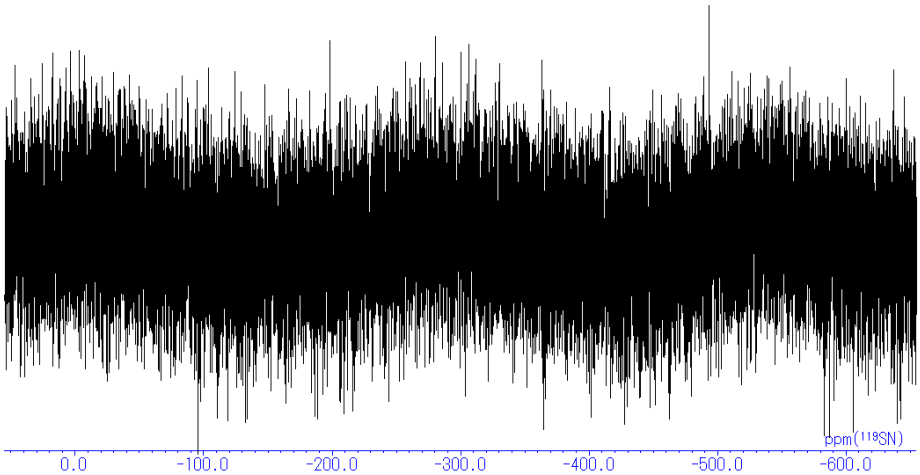

Chart S15. ^{119}Sn NMR spectrum of **TAz-PPV-C8** in $CDCl_3$.

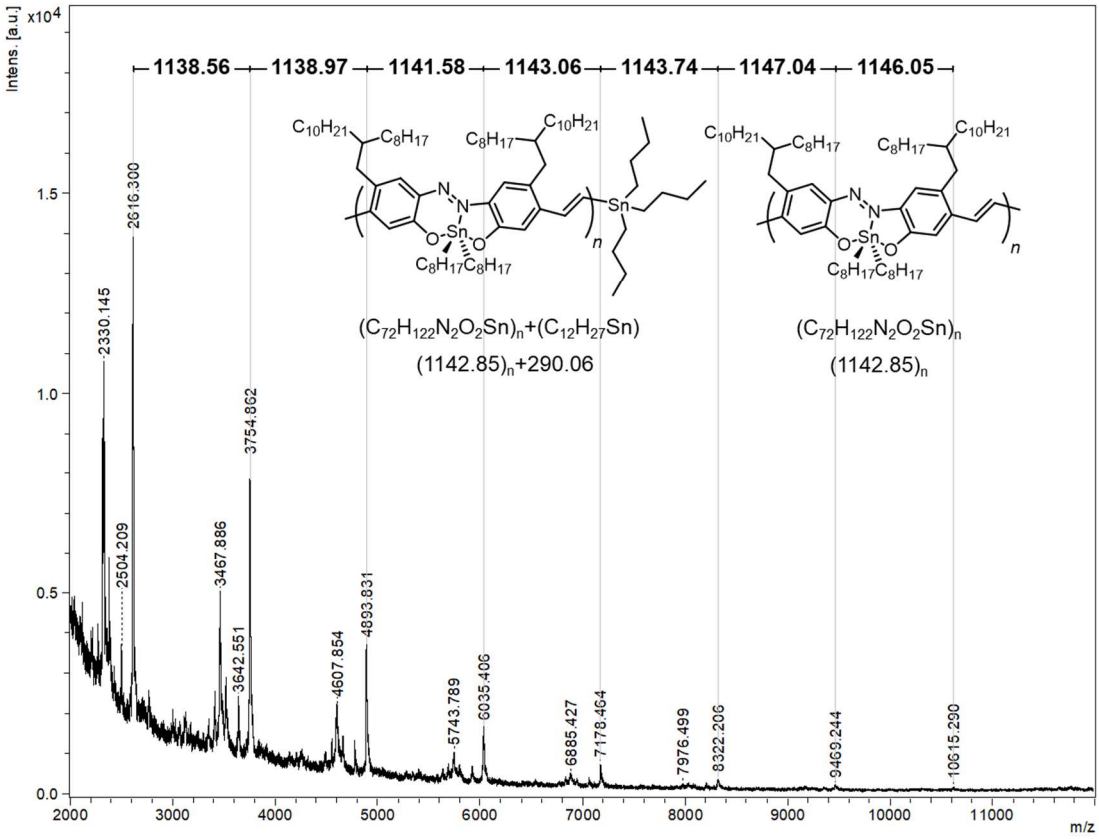

Chart S16. MADLI-TOF MS spectrum of **TAz-PPV-C8**.

Synthesis of Model Compounds

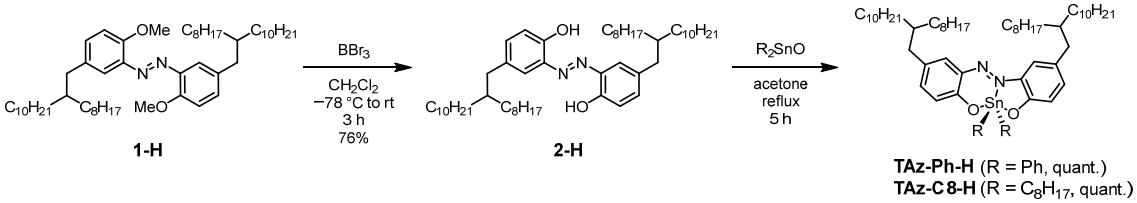

Synthesis of **2-H**

Compound **1-H** (0.700 g, 0.871 mmol, 1 equiv.) was placed in a round-bottom flask equipped with a magnetic stirring bar. After degassing and filling N_2 three times, CH_2Cl_2 (15 mL) was added to the flask. After cooling the mixture to −78 °C, BBr_3 (1 M in CH_2Cl_2, 4.36 mL, 4.36 mmol, 5 equiv.) was dropwise added. The reaction was carried out at room temperature for 3 h. After the reaction, MeOH was carefully added at 0 °C for quenching the reaction and the solvent was removed with a rotary evaporator. The residue was purified by column chromatography on SiO_2 (hexane/CH_2Cl_2 = 3/1 v/v as an eluent) to afford **2-H** (0.512 g, 0.660 mmol, 76%) as an orange oil.

R_f = 0.75 (hexane/CH_2Cl_2 = 3/1 v/v). ^{1}H NMR ($CHCl_3$, 400 MHz) δ 12.19 (s, 2H), 7.46 (d, J = 2.1 Hz, 2H), 7.14 (d, J = 2.1 Hz, 2H), 7.14 (d, J = 2.0 Hz, 2H), 6.95 (d, J = 8.4 Hz, 2H), 2.54 (d, J = 7.3 Hz, 2H), 1.25 (br, 64H), 0.88 (m, 14H) ppm; ^{13}C{^{1}H} NMR ($CDCl_3$, 100 MHz) δ 150.9, 134.8, 134.1, 133.8, 131.1, 118.1, 39.7, 39.5, 33.1, 31.9, 30.0, 29.7, 29.7, 29.6, 29.6, 29.3, 29.3, 26.6, 22.7, 14.1 ppm; HRMS (ESI) calcd. for $C_{52}H_{89}N_2O_2$ $[M-H]^-$: 773.6930, found: 773.6938.

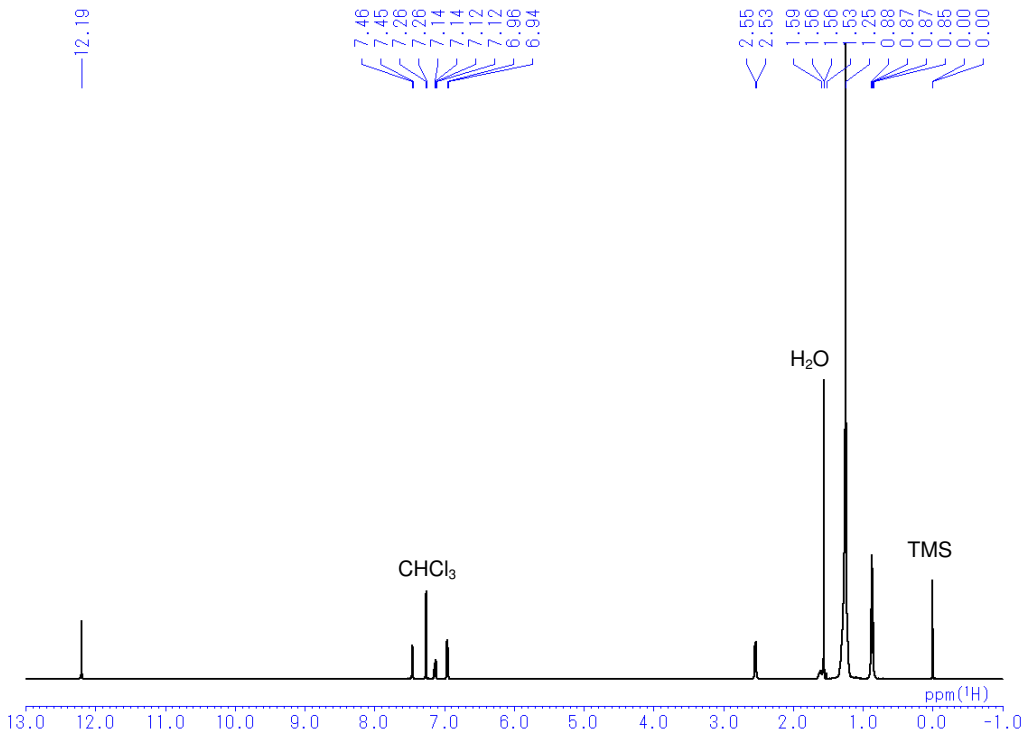

Chart S17. ^{1}H NMR spectrum of **2-H** in $CDCl_3$.

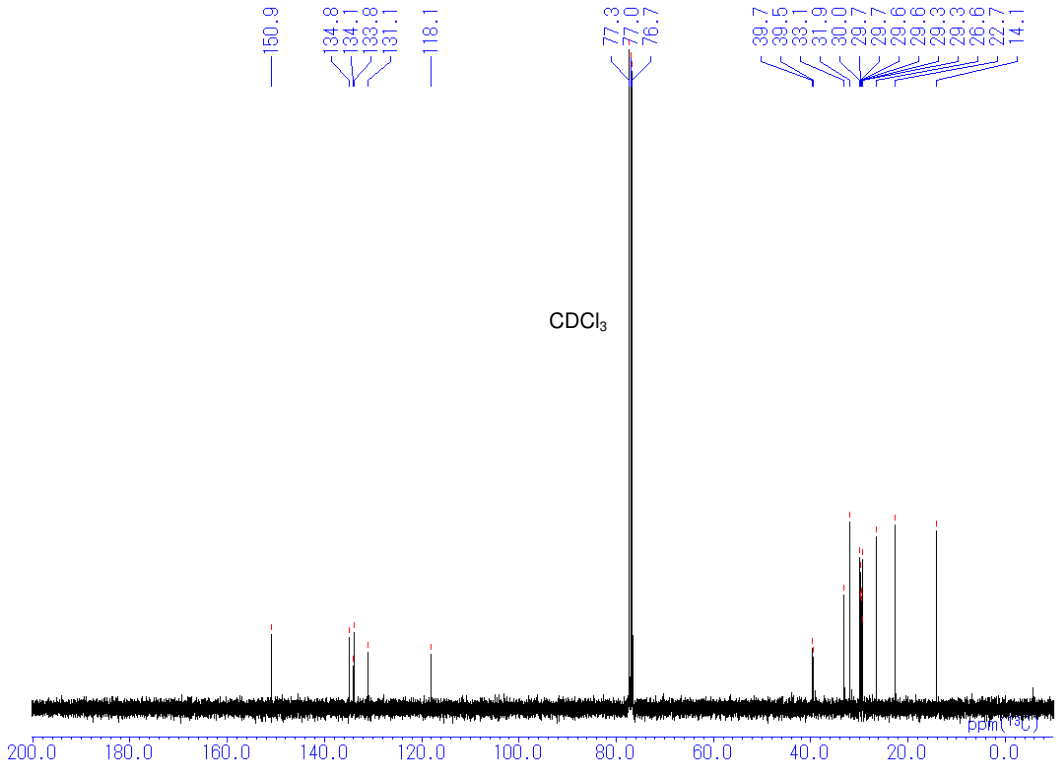

Chart S18. ^{13}C{^{1}H} NMR spectrum of **2-H** in $CDCl_3$.

Synthesis of **TAz-Ph-H**

In a 20 mL round bottom flask, **2-H** (0.114 g, 0.147 mmol, 1 equiv.), diphenyltin(IV) oxide (0.0637 g, 0.221 mmol, 1.5 equiv.) and 5 mL of acetone were added under N_2. Then, the solution was stirred at reflux temperature for 5 h. Insoluble products were filtered, and the solution was concentrated *in vacuo* to give **TAz-Ph-H** (0.154 g, 0.147 mmol, quant.) as a violet oil.

^{1}H NMR ($CHCl_3$, 400 MHz) δ 7.90 (m, 4H), 7.50 (d, J = 2.0 Hz, 1H), 7.41–7.38 (m, 6H), 7.35 (d, J = 2.2 Hz, 1H), 7.19–7.15 (m, 2H), 7.01–6.98 (m, 2H), 2.49–2.44 (m, 4H), 1.25 (br, 64H), 0.88–0.84 (m, 14H) ppm; ^{13}C{^{1}H} NMR ($CDCl_3$, 100 MHz) δ 160.1, 159.1, 139.5, 138.0, 137.2, 136.5 136.4, 135.6, 134.7, 131.8, 131.8, 130.4, 128.8, 123.1, 119.7, 116.6 39.9, 39.6, 39.5, 39.3, 33.1, 31.9, 31.9, 30.0, 29.7, 29.7, 29.6, 29.6, 29.3, 29.3, 26.6, 26.6, 22.7, 14.1 ppm; ^{119}Sn NMR ($CDCl_3$, 149 MHz) δ –364.3 ppm: HRMS (ESI) calcd. for $C_{64}H_{99}N_2O_2Sn$ $[M+H]^+$: 1047.6723, found: 1067.6738.

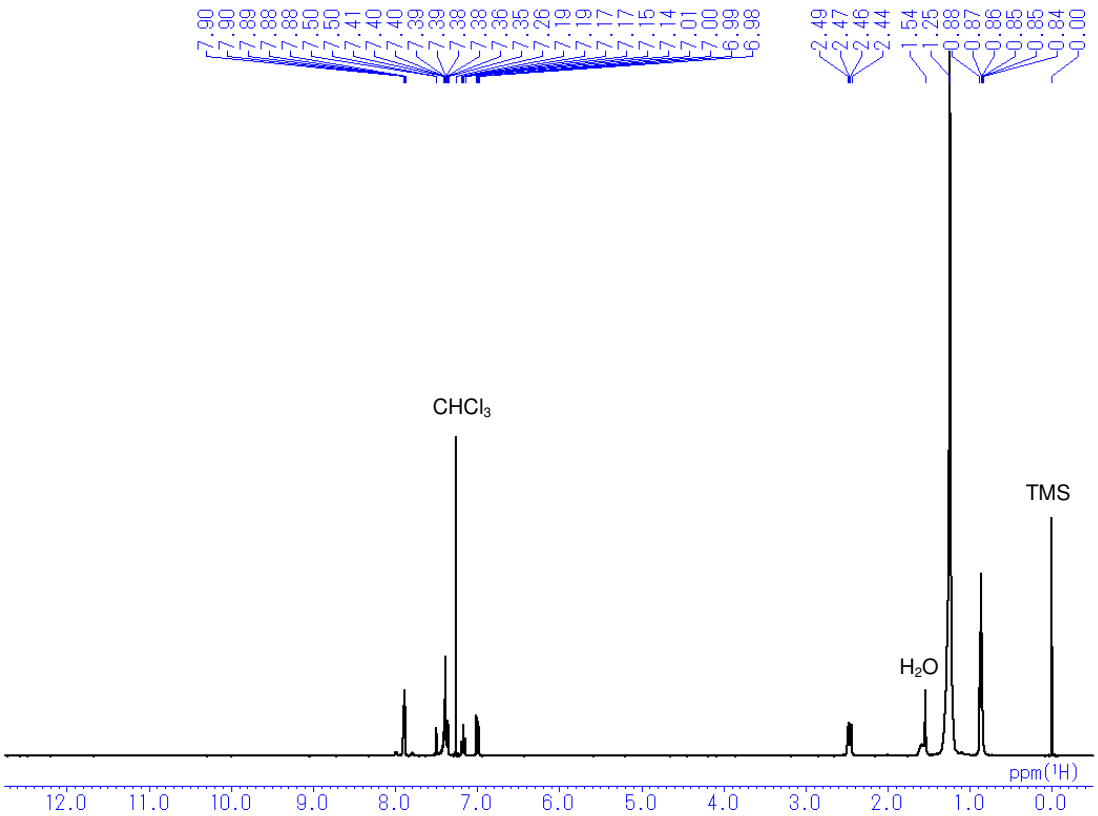

Chart S19. ^{1}H NMR spectrum of **TAz-Ph-H** in $CDCl_3$.

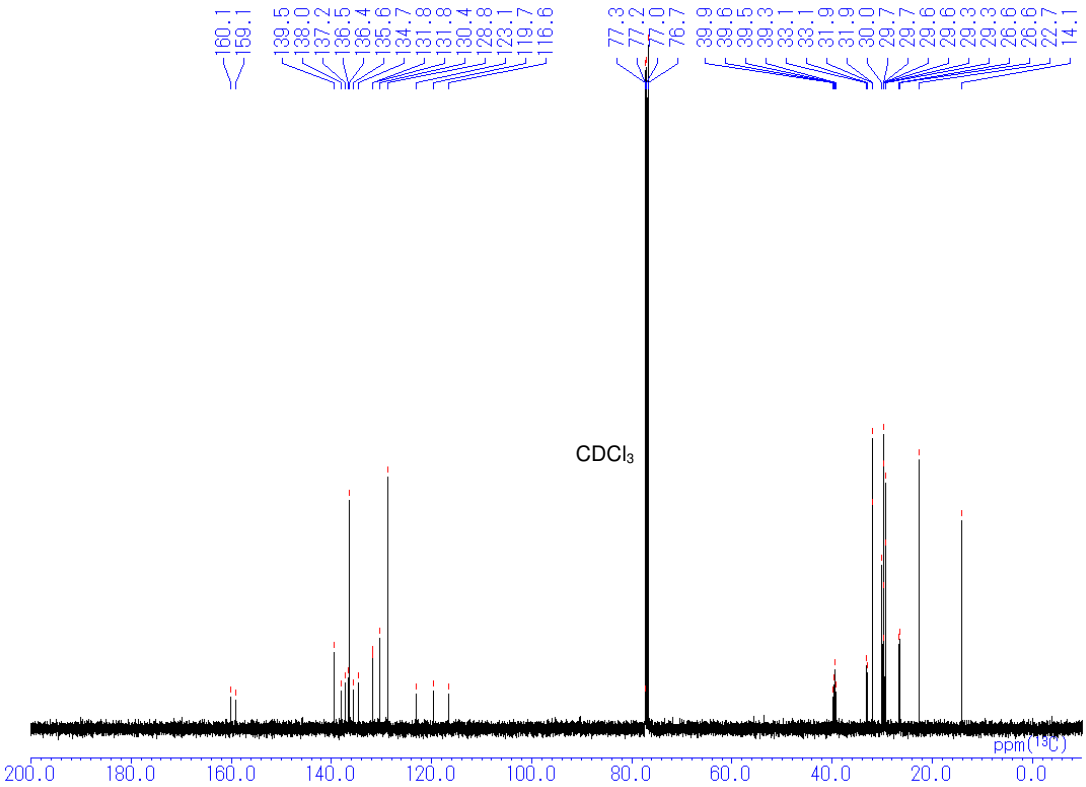

Chart S20. $^{13}C\{^{1}H\}$ NMR spectrum of **TAz-Ph-H** in $CDCl_3$.

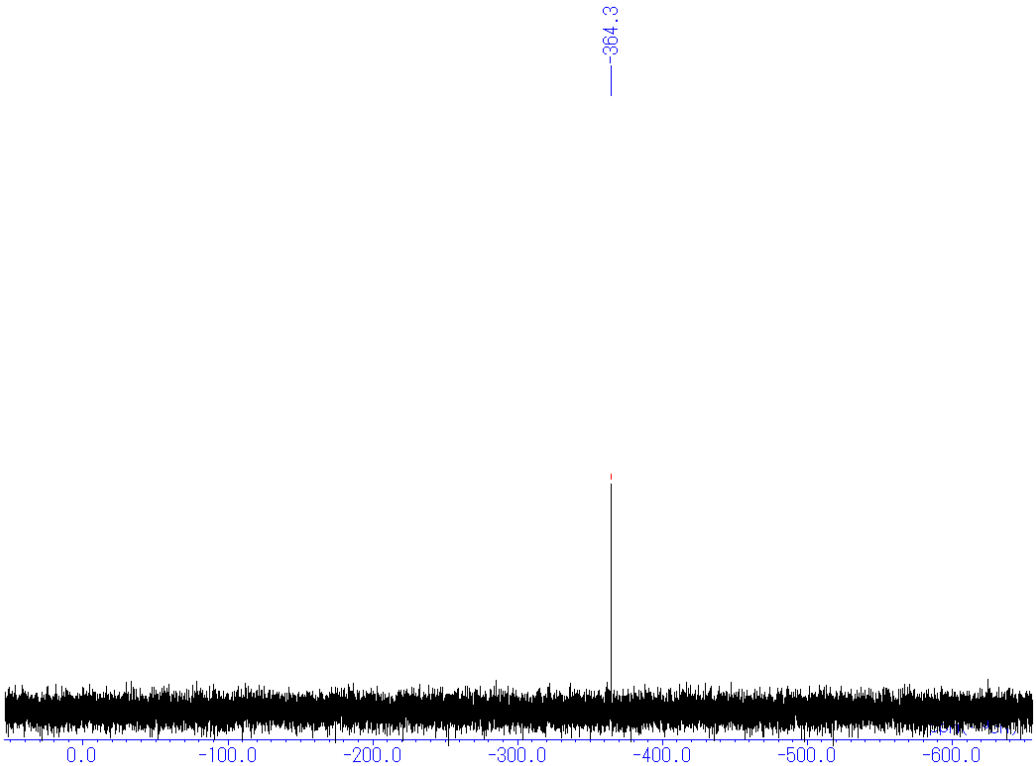

Chart S21. ^{119}Sn NMR spectrum of **TAz-Ph-H** in $CDCl_3$.

Synthesis of **TAz-C8-H**

In a 20 mL round bottom flask, **2-H** (0.129 g, 0.166 mmol, 1 equiv.), dioctyltin(IV) oxide (0.0901 g, 0.250 mmol, 1.5 equiv.) and 5 mL of acetone were added under N_2. Then, the solution was stirred at reflux temperature for 5 h. Insoluble products were filtrated and the solution was concentrated *in vacuo* to give **TAz-C8-H** (0.185 g, 0.166 mmol, quant.) as a violet oil.

^{1}H NMR ($CHCl_3$, 400 MHz) δ 7.50 (d, J = 1.8 Hz, 1H), 7.33 (d, J = 2.2 Hz, 1H), 7.11–7.06 (m, 2H), 6.74 (d, J = 8.5 Hz, 1H), 6.69 (d, J = 8.5 Hz, 1H) 2.48–2.45 (m, 4H), 1.65–1.47 (br, 2H), 1.25 (br, 92H), 0.89–0.83 (m, 18H) ppm; ^{13}C{^{1}H} NMR ($CDCl_3$, 100 MHz) δ 160.6, 158.8, 137.5, 137.3, 136.9, 135.4, 135.4, 134.3, 131.2, 122.8, 119.3, 116.6, 39.8, 39.5, 39.5, 39.3, 33.5, 33.1, 33.1, 31.9, 31.8, 31.7, 30.1, 29.7, 29.7, 29.7, 29.4, 29.3, 29.1, 29.0, 26.6, 26.6, 24.8, 22.8, 22.7, 22.6, 22.6, 14.1, 14.1 ppm; ^{119}Sn NMR ($CDCl_3$, 149 MHz) δ −221.2 ppm: HRMS (ESI) calcd. for $C_{68}H_{123}N_2O_2Sn$ $[M+H]^+$: 1119.8601, found: 1119.8635.

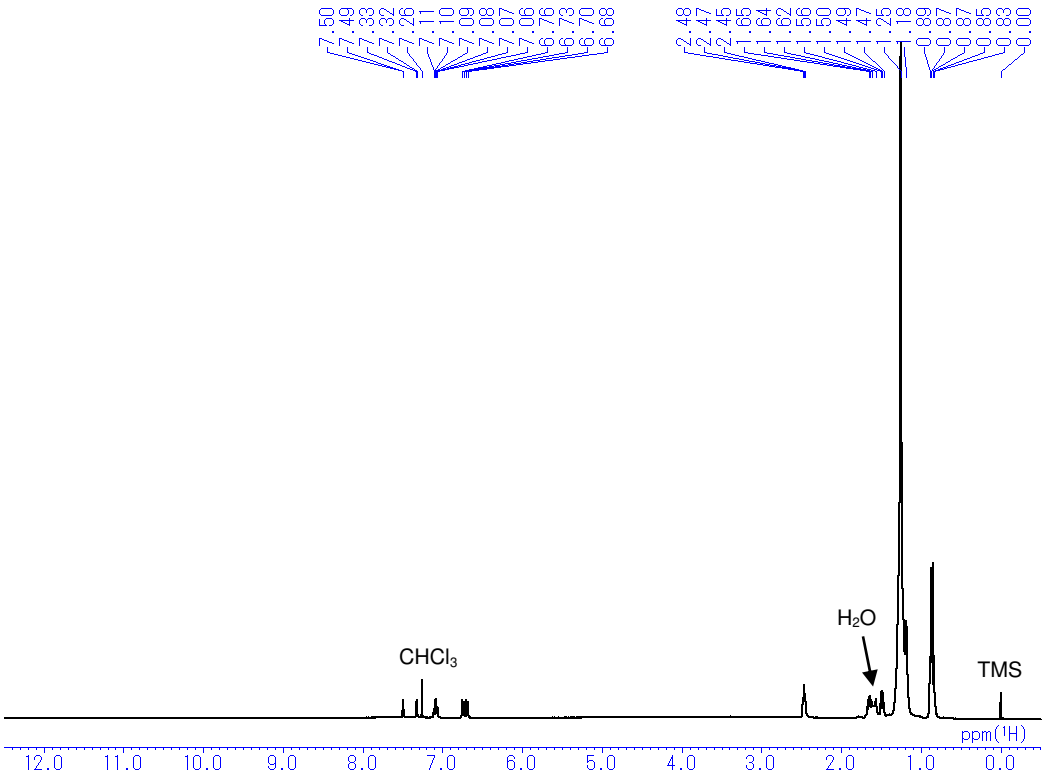

Chart S22. ^{1}H NMR spectrum of **TAz-C8-H** in $CDCl_3$.

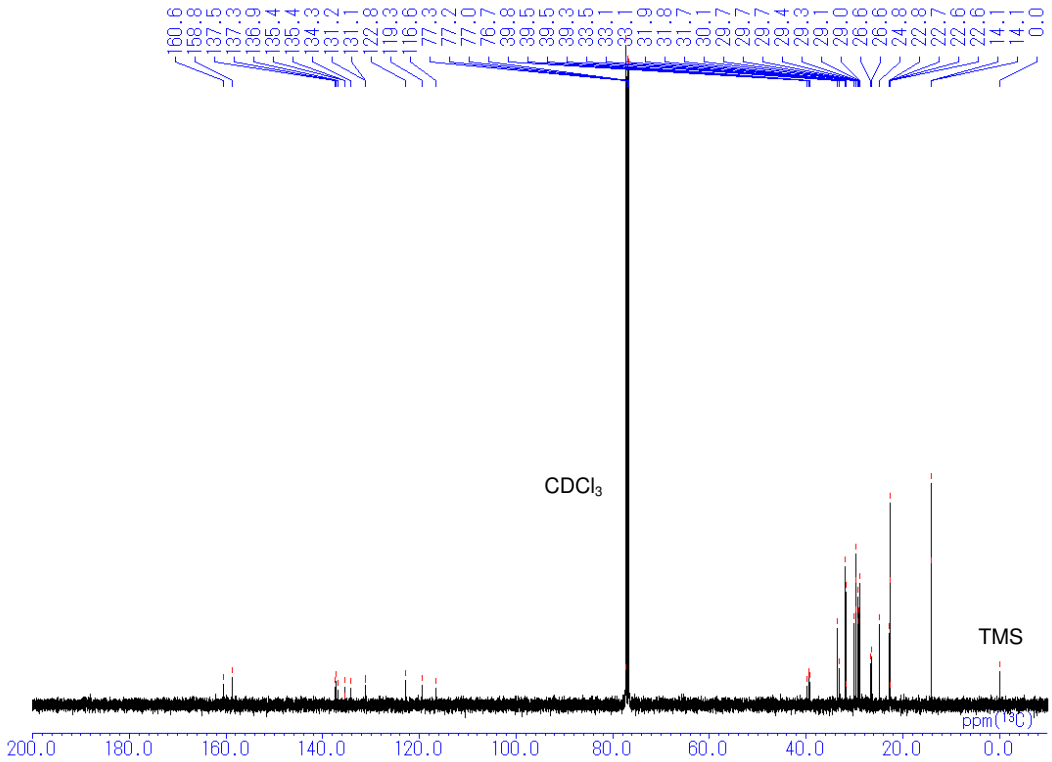

Chart S23. $^{13}C\{^{1}H\}$ NMR spectrum of **TAz-C8-H** in $CDCl_3$.

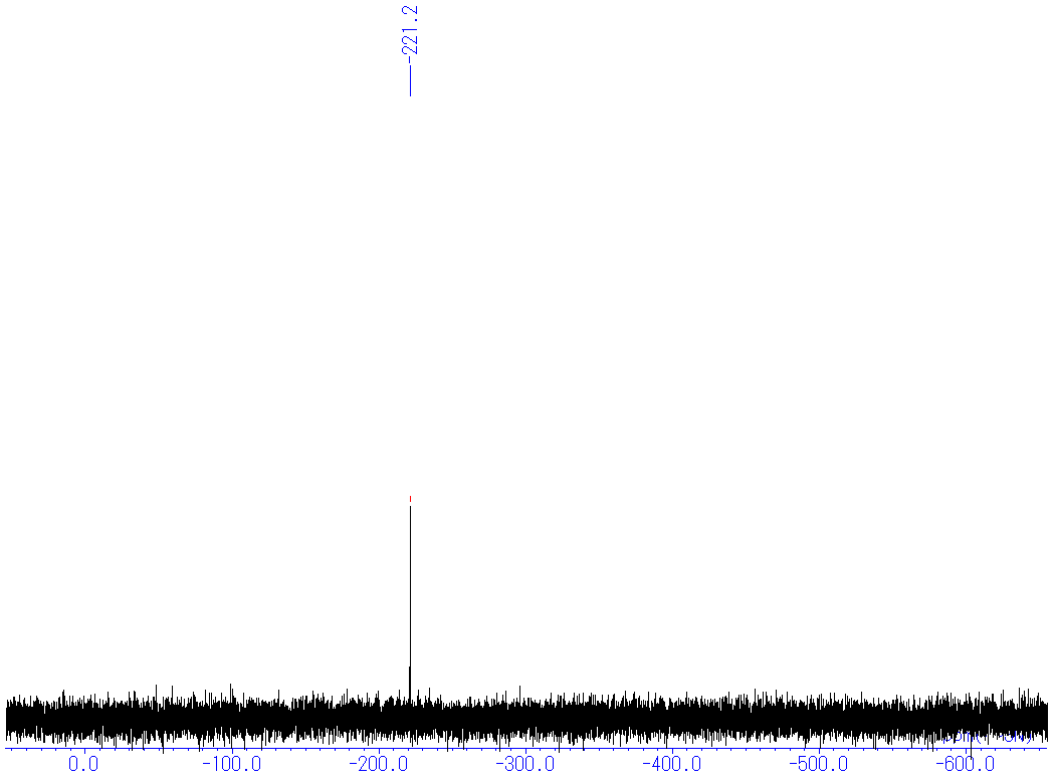

Chart S24. ^{119}Sn NMR spectrum of **TAz-C8-H** in $CDCl_3$.

GPC chromatograms and properties of polymers

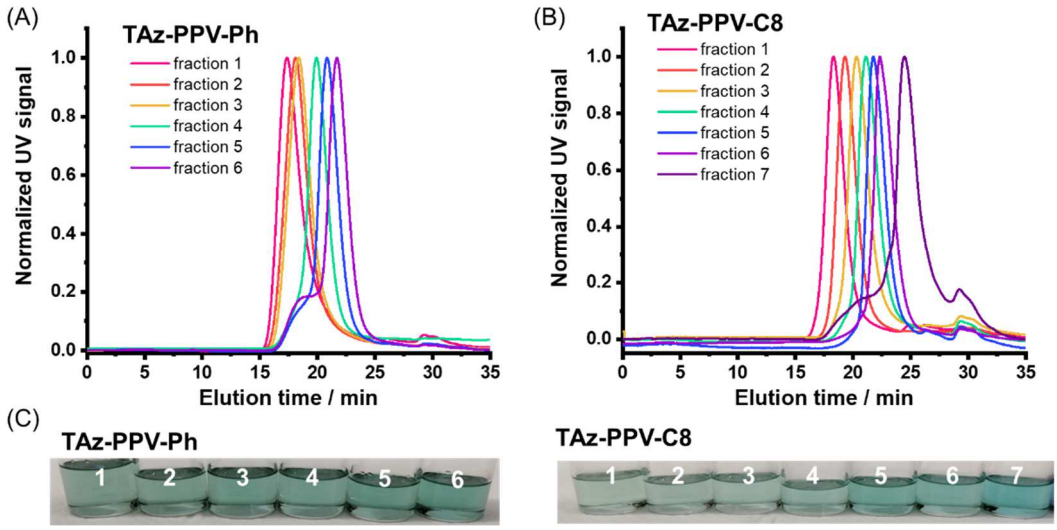

Figure S1. Gel permeation chromatography (GPC) profiles of (A) **TAz-PPV-Ph** and (B) **TAz-PPV-C8**. Molecular weights were evaluated with chloroform as an eluent (1.0 mL / min) at 40 °C. (C) Photographs of fractionated samples under room light (the numbers denote fraction numbers).

Table S1. Properties of fractionated **TAz-PPV-Ph** by HPLC

Fraction	1	2	3	4	5	6
M_n /kDa [a]	41	33	19	12	8.3	6.0
n [b]	39	31	18	11	7.8	5.6
PDI [a]	2.2	1.7	1.5	1.5	1.4	2.0

[a] Determined by GPC with polystyrene standards (PDI: poly dispersity index, M_w/M_n).

[b] Degree of polymerization ($n = M_n/M$(repeating unit)).

Table S2. Properties of fractionated **TAz-PPV-C8** by HPLC

Fraction	1	2	3	4	5	6	7
M_n /kDa [a]	29	16	8.8	6.2	4.2	3.2	2.2
n [b]	25	14	7.7	5.4	3.7	2.8	1.9
PDI [a]	1.4	1.2	1.3	1.2	1.2	1.3	1.2

[a] Determined by GPC with polystyrene standards (PDI: poly dispersity index, M_w/M_n).

[b] Degree of polymerization ($n = M_n/M$(repeating unit)).

Molecular models of TAz and BAz complexes

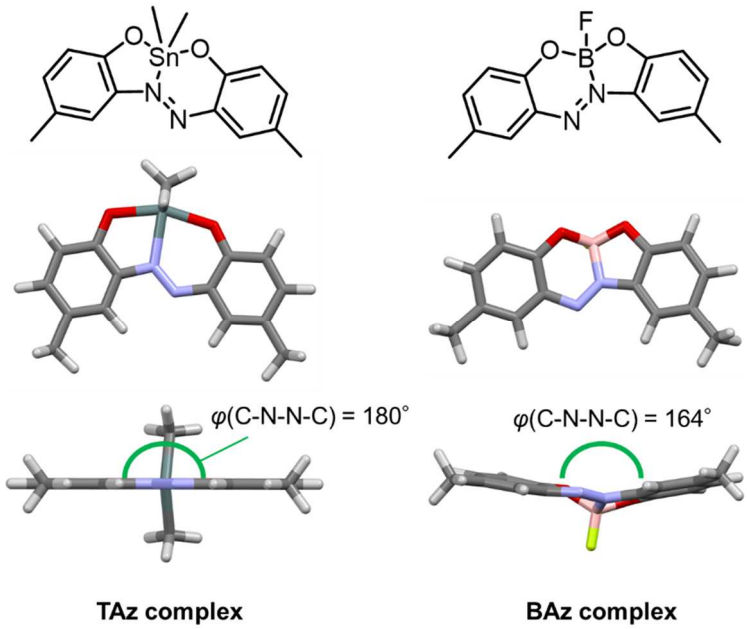

Figure S2. Molecular models and dihedral angles (C-N-N-C) of TAz and BAz complexes by DFT calculation at B3LYP/6-31G(d,p) for C, H, N, O, B and LanL2DZ for Sn levels. The calculation details are described below section. Hydrogen atoms were omitted for clarity.

Cyclic voltammograms

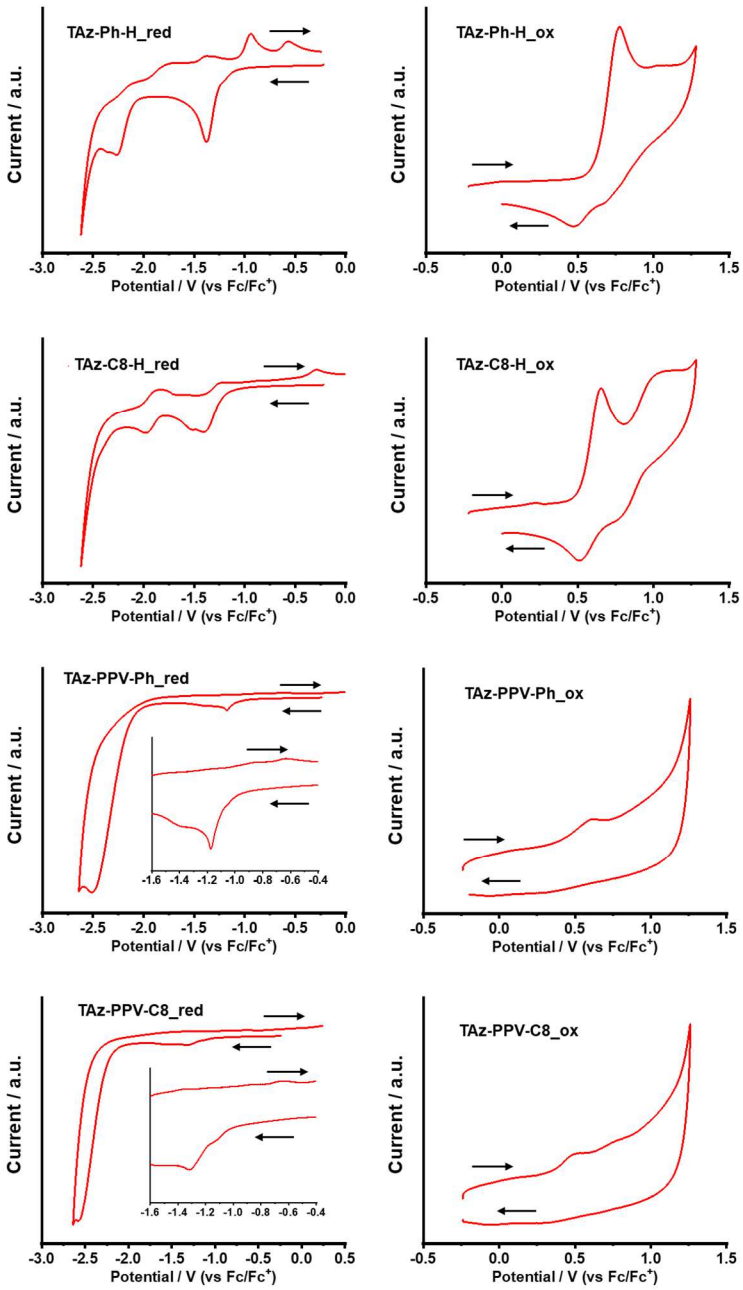

Figure S3. Cyclic voltammograms (red: reduction, negative sweep, ox: oxidation, positive sweep) of **TAz-Ph-H**, **TAz-C8-H**, **TAz-PPV-Ph**, **TAz-PPV-C8** in CH_2Cl_2 (1.0×10^{-3} M, 1.0×10^{-3} M per repeating unit for the polymers) containing $N^nBu_4PF_6$ (0.10 M) using a glassy carbon (GC) working electrode, a Pt wire counter electrode, an Ag/AgCl reference electrode, and a Fc/Fc^+ external standard at room temperature with a scan rate of 0.1 V s^{-1}. The arrow denotes sweep direction.

Computational details for theoretical calculation

The Gaussian 16 program package[2] was used for computation. We optimized the structures of the monomers (M), dimers (D), and trimers (T) of **TAz-PPV-Ph′** and **TAz-PPV-C8′** in the ground S_0 states and calculated their molecular orbitals, respectively. **TAz-PPV-Ph′** and **TAz-PPV-C8′** were model compounds of **TAz-PPV-Ph** and **TAz-PPV-C8** in which the long alkyl chains (2-octyldodecyl and octyl groups) were replaced with methyl groups to reduce calculation cost for precise evaluation of expanded π-conjugated system. All calculations with density functional theory (DFT) and time-dependent (TD) DFT were carried out at B3LYP/6-31G(d,p) for C, H, N, O, B and LanL2DZ for Sn levels. The DFT and TD-DFT were applied for the optimization of the structures in the S_0 and S_1 states, respectively. We calculated the energy of the S_0–S_1 transitions with optimized geometries in the S_0 and S_1 states by TD-DFT. We newly calculated the energy of molecular orbitals (MOs) of **BAz-PPV** in the S_0 states to compare the results of **TAz-PPV** with those of **BAz-PPV** in our previous work[1].

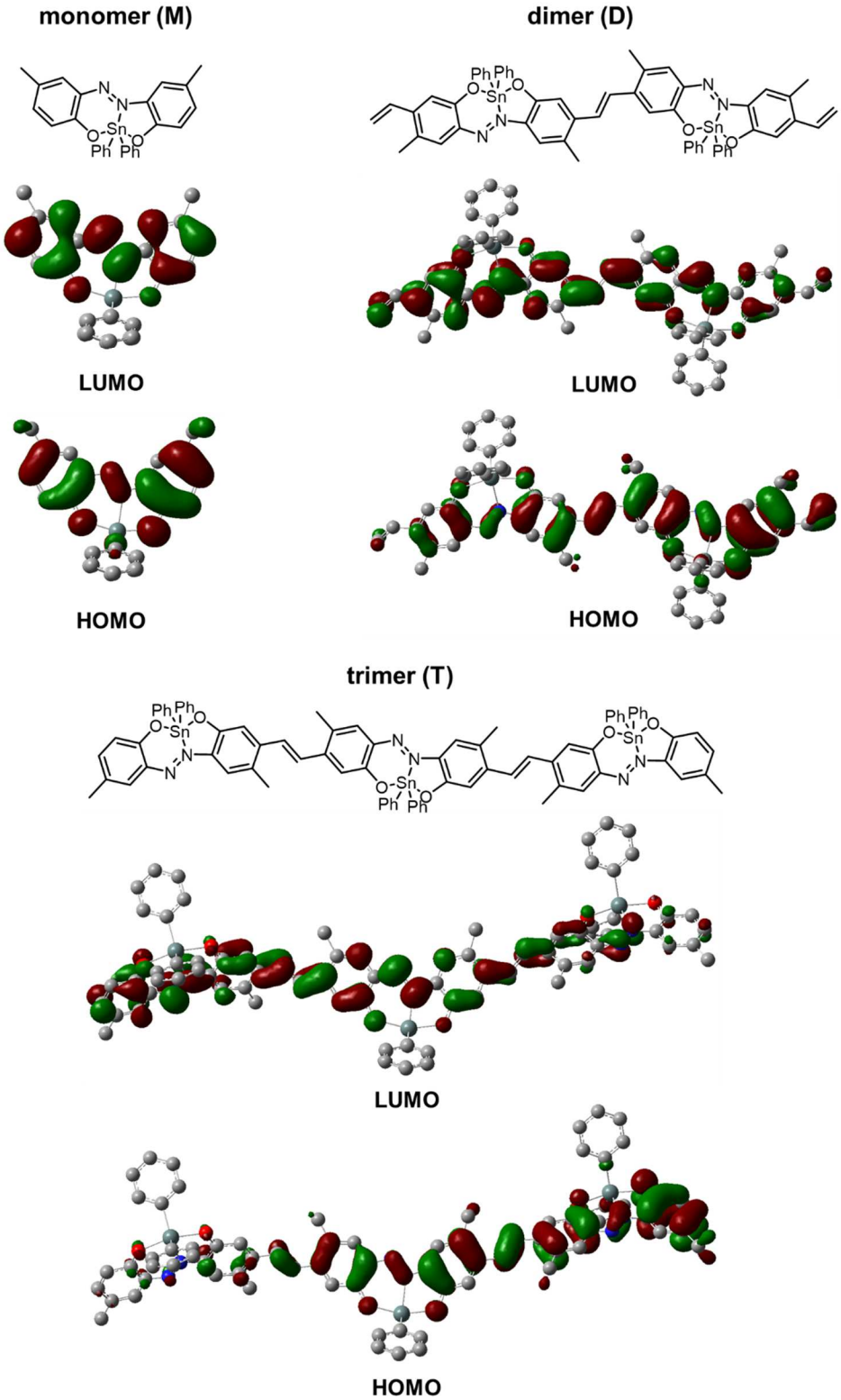

Figure S4. Chemical structures Kohn–Sham orbitals in monomers (M), dimers (D) and trimers (T) of **TAz-PPV-Ph′**. Hydrogen atoms were omitted for clarity.

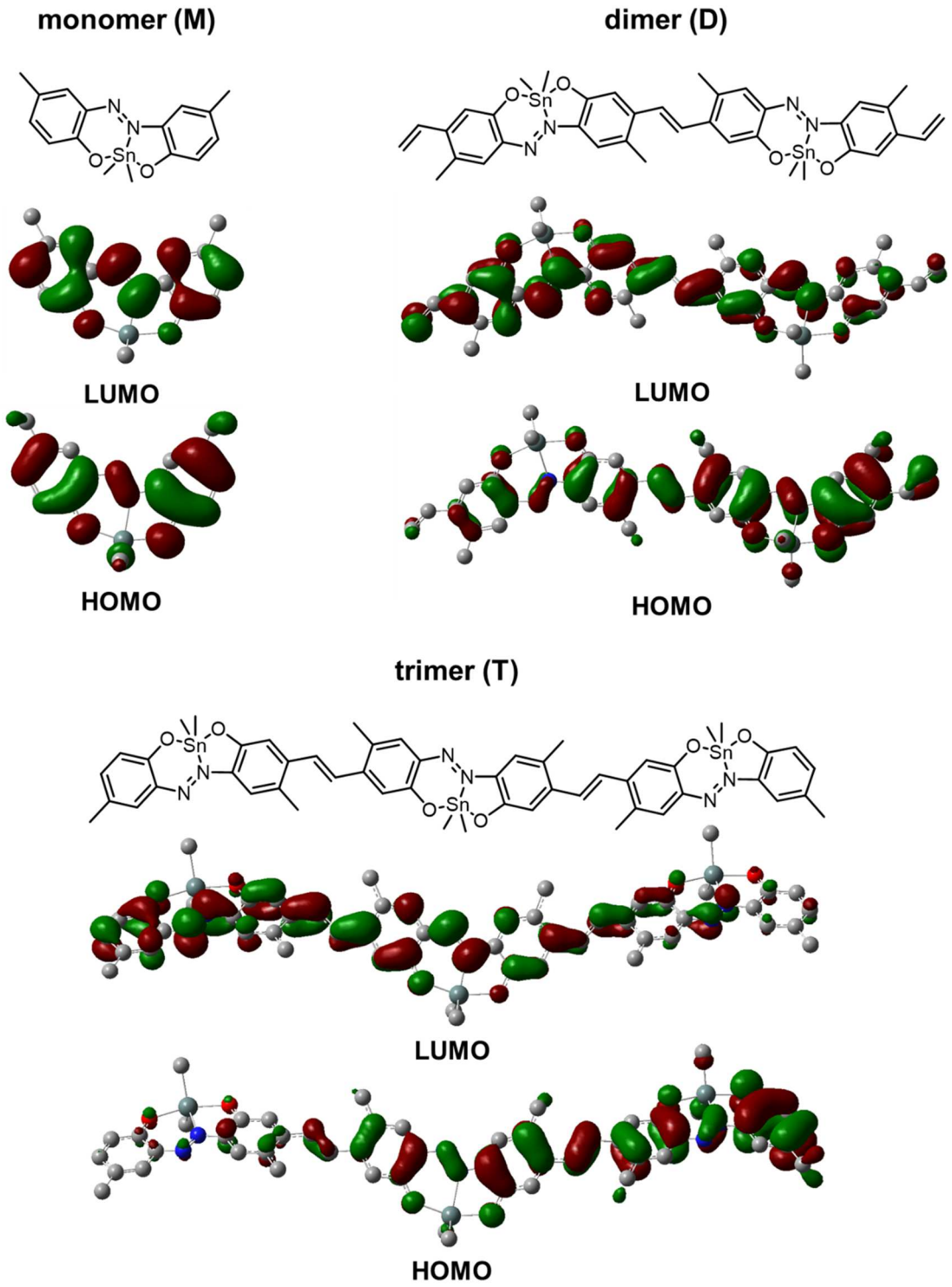

Figure S5. Chemical structures and Kohn–Sham orbitals in monomers (M), dimers (D) and trimers (T) of **TAz-PPV-C8′**. Hydrogen atoms were omitted for clarity.

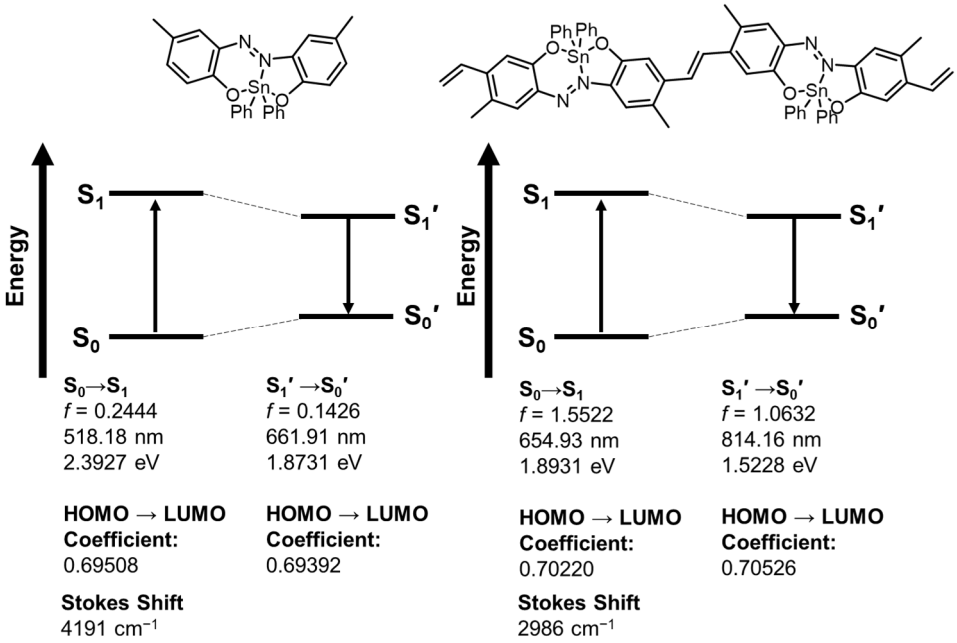

Figure S6. Energy diagrams of absorption and emission in monomer and dimer of **TAz-PPV-Ph′** in the ground and excited states.

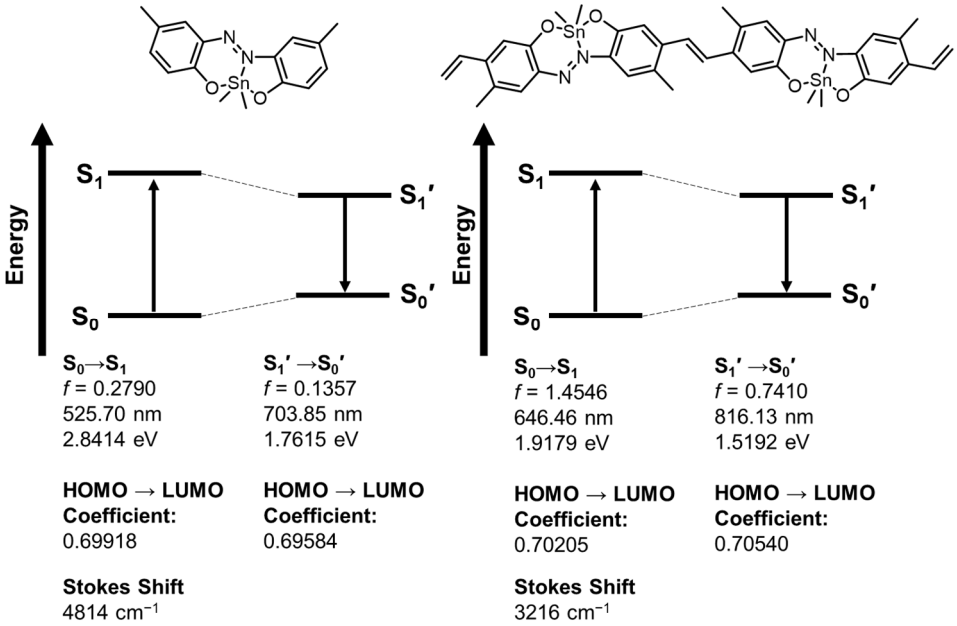

Figure S7. Energy diagrams of absorption and emission in monomer and dimer of **TAz-PPV-C8′** in the ground and excited states.

Table S3. Results of representative transitions of TAz monomers (M) and dimers (D) from TD-DFT calculations

	Energy gap / eV	**Wavelength / nm**	**Oscillator Strength**	**transition**	**Assignment (Coefficient)**
TAz-PPV-Ph′					
M	2.3927	518.18	0.2444	$S_0 \rightarrow S_1$	HOMO → LUMO (0.69508)
	3.4404	360.38	0.2704	$S_0 \rightarrow S_4$	HOMO−2 → LUMO (0.68932)
D	1.8931	654.93	1.5522	$S_0 \rightarrow S_1$	HOMO → LUMO (0.70220)
	2.6099	475.04	0.2746	$S_0 \rightarrow S_6$	HOMO−3 → LUMO (0.63594)
	2.7181	456.14	0.3452	$S_0 \rightarrow S_7$	HOMO−4 → LUMO (0.64072)
TAz-PPV-C8′					
M	2.3584	525.70	0.2790	$S_0 \rightarrow S_1$	HOMO → LUMO (0.69598)
	3.4448	359.92	0.2849	$S_0 \rightarrow S_4$	HOMO−2 → LUMO (0.69024)
D	1.9179	646.46	1.4546	$S_0 \rightarrow S_1$	HOMO → LUMO (0.70205)
	2.6166	473.84	0.3552	$S_0 \rightarrow S_6$	HOMO−3 → LUMO (0.63863)
	2.7409	452.36	0.3808	$S_0 \rightarrow S_7$	HOMO−4 → LUMO (0.63845)

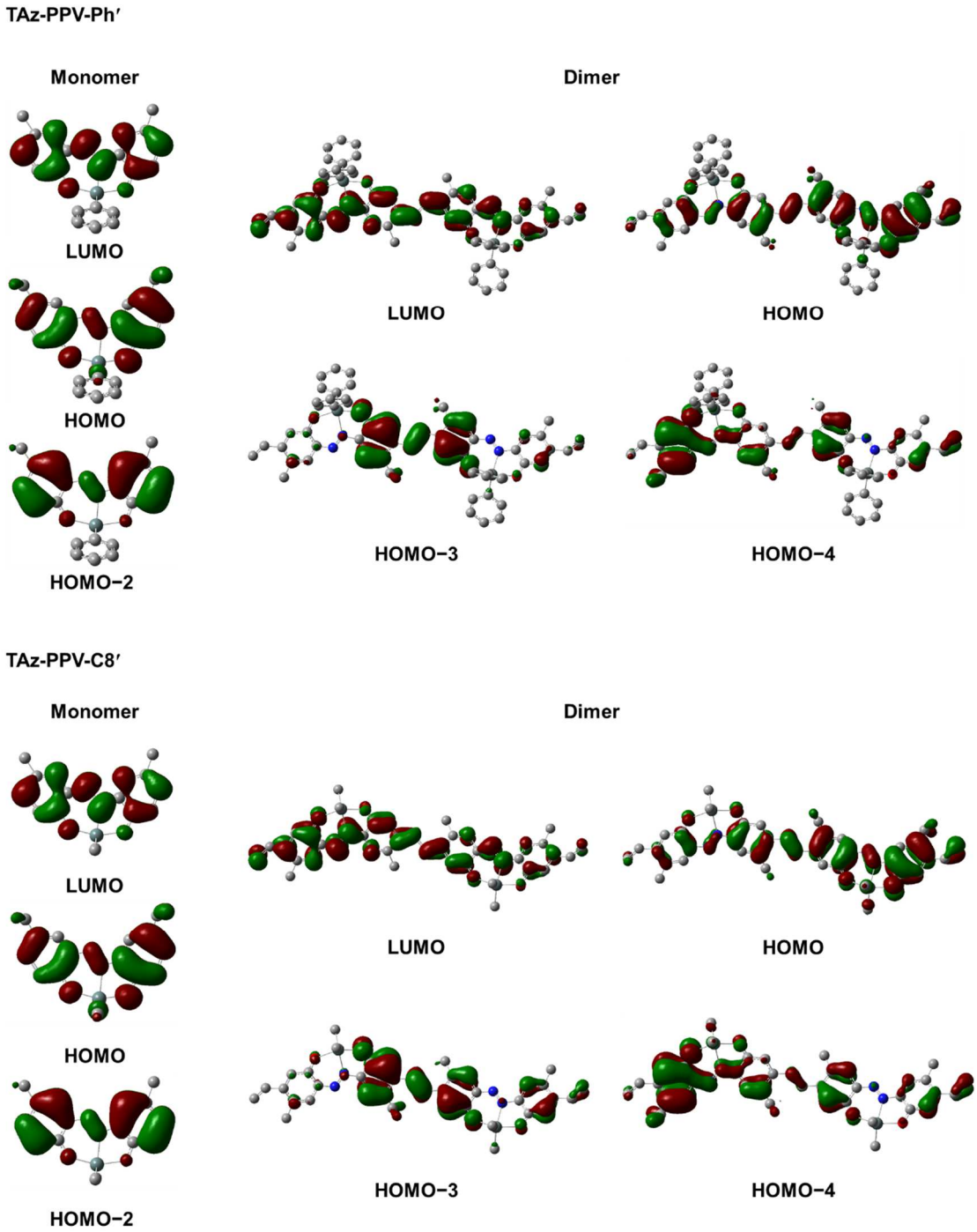

Figure S8. Selected Kohn–Sham orbitals for Table S3 in monomers (M), dimers (D) of **TAz-PPV-Ph′** and **TAz-PPV-C8′**. Hydrogen atoms were omitted for clarity.

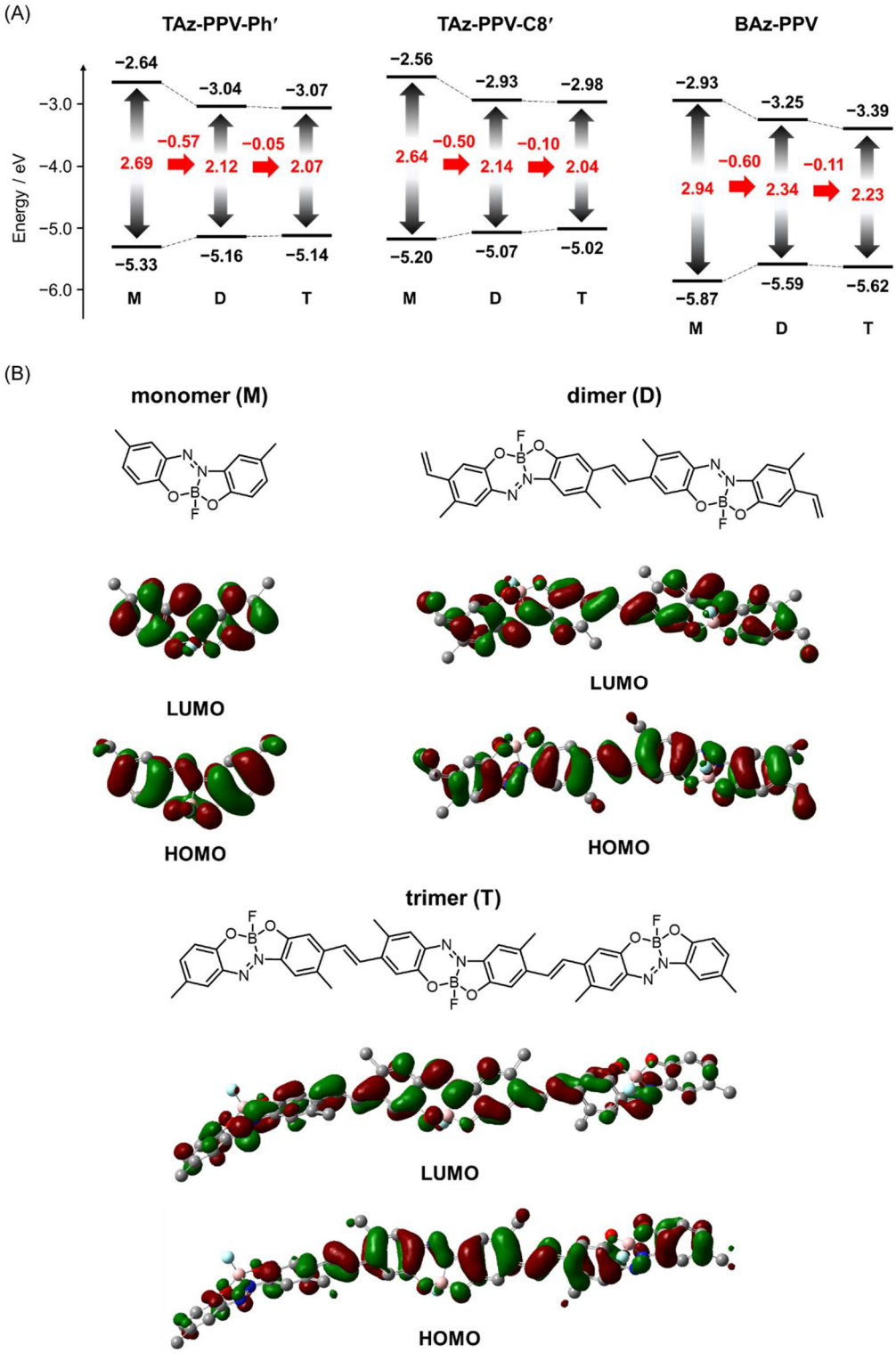

Figure S9. (A) Energy levels and energy gaps of HOMOs and LUMOs of **TAz-PPV-Ph′**, **TAz-PPV-C8′** and **BAz-PPV**. (B) Chemical structures and Kohn–Sham orbitals in monomers (M), dimers (D) and trimers (T) of **BAz-PPV**. Hydrogen atoms were omitted for clarity.

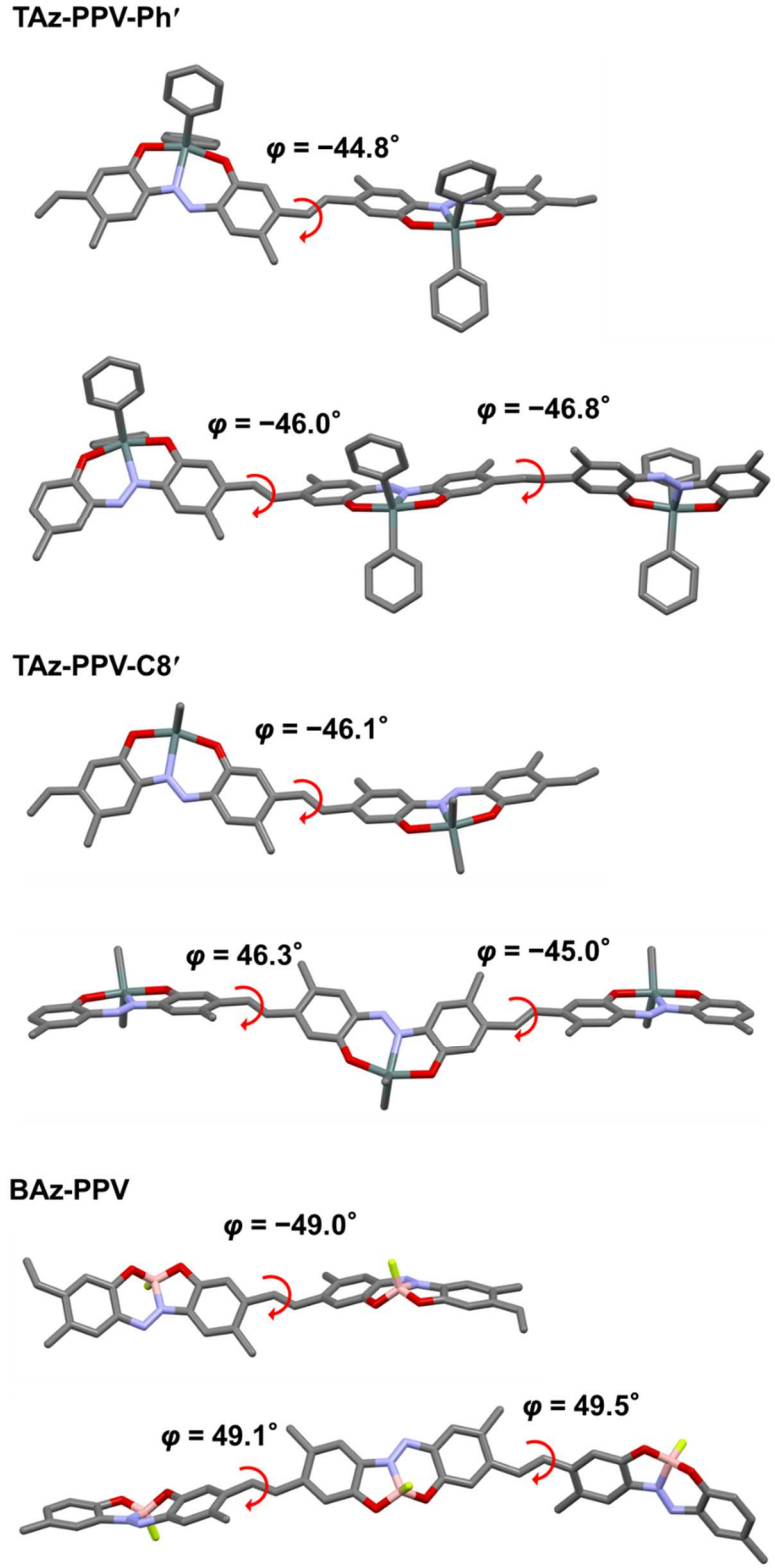

Figure S10. Dihedral angles between benzene rings of adjacent units of dimers and trimers of **TAz-PPV-Ph′**, **TAz-PPV-C8′** and **BAz-PPV**. Hydrogen atoms were omitted for clarity.

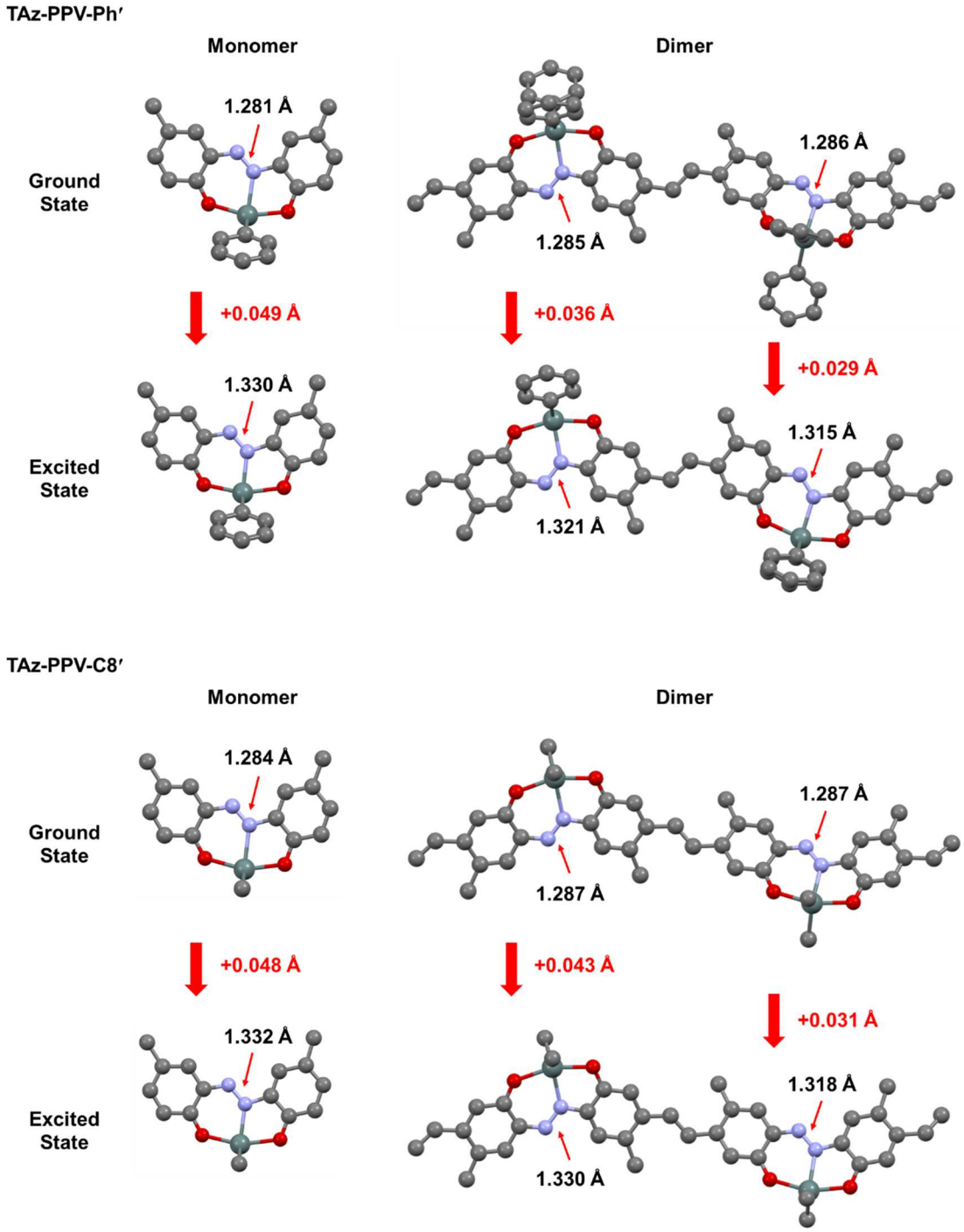

Figure S11. Optimized structures and N=N bond lengths in the ground and excited states of monomers and dimers of **TAz-PPV-Ph′** and **TAz-PPV-C8′**. Hydrogen atoms were omitted for clarity.

Reference

1. Wakabayashi J, Gon M, Tanaka K, Chujo Y. Near-Infrared Absorptive and Emissive Poly(*p*-phenylene vinylene) Derivative Containing Azobenzene–Boron Complexes. Macromolecules. 2020;53:4524–32.
2. Gaussian 16, Revision C.01, Frisch MJ, Trucks GW, Schlegel HB, Scuseria GE, Robb MA, Cheeseman JR, Scalmani G, Barone V, Petersson GA, Nakatsuji H, Li X, Caricato M, Marenich AV, Bloino J, Janesko BG, Gomperts R, Mennucci B, Hratchian HP, Ortiz JV, Izmaylov AF, Sonnenberg JL, Williams-Young D, Ding F, Lipparini F, Egidi F, Goings J, Peng B, Petrone A, Henderson T, Ranasinghe D, Zakrzewski VG, Gao J, Rega N, Zheng G, Liang W, Hada M, Ehara M, Toyota K, Fukuda R, Hasegawa J, Ishida M, Nakajima T, Honda Y, Kitao O, Nakai H, Vreven T, Throssell K, Montgomery JA Jr, Peralta JE, Ogliaro F, Bearpark MJ, Heyd JJ, Brothers EN, Kudin KN, Staroverov VN, Keith TA, Kobayashi R, Normand J, Raghavachari K, Rendell AP, Burant JC, Iyengar SS, Tomasi J, Cossi M, Millam JM, Klene M, Adamo C, Cammi R, Ochterski JW, Martin RL, Morokuma K, Farkas O, Foresman JB, Fox DJ. Gaussian, Inc., Wallingford CT, 2016.